AFRL-RX-TY-TR-2010-0038

COMPUTATIONAL FLOW ANALYSIS OF ULTRA HIGH PRESSURE FIREFIGHTING TECHNOLOGY WITH APPLICATION TO LONG RANGE NOZZLE DESIGN

Christopher P. Menchini
Applied Research Associates, Inc.
P.O. Box 40128
Tyndall Air Force Base, FL 32403

Contract: FA4819-07-D-0001

MARCH 2010

AIR FORCE RESEARCH LABORATORY
MATERIALS AND MANUFACTURING DIRECTORATE

■ **Air Force Materiel Command** ■ **United States Air Force** ■ **Tyndall Air Force Base, FL 32403-5323**

NOTICE AND SIGNATURE PAGE

Using Government drawings, specifications, or other data included in this document for any purpose other than Government procurement does not in any way obligate the U.S. Government. The fact that the Government formulated or supplied the drawings, specifications, or other data does not license the holder or any other person or corporation; or convey any rights or permission to manufacture, use, or sell any patented invention that may relate to them.

This report was cleared for public release by the Air Force Research Laboratory, Materials and Manufacturing Directorate, Airbase Technologies Division, Public Affairs and is available to the general public, including foreign nationals. Copies may be obtained from the Defense Technical Information Center (DTIC) (http://www.dtic.mil).

REPORT NUMBER AFRL-RX-TY-TR-2010-0038 HAS BEEN REVIEWED AND IS APPROVED FOR PUBLICATION IN ACCORDANCE WITH ASSIGNED DISTRIBUTION STATEMENT.

//signature//
R. CRAIG MELLERSKI, DR-III
Work Unit Manager

//signature//
SANDRA R. MEEKER, DR-IV
Chief, Deployed Base Systems Branch

//signature//
ALBERT N. RHODES, PhD
Acting Chief, Airbase Technologies Division

This report is published in the interest of scientific and technical information exchange, and its publication does not constitute the Government's approval or disapproval of its ideas or findings.

REPORT DOCUMENTATION PAGE

Form Approved
OMB No. 0704-0188

PLEASE DO NOT RETURN YOUR FORM TO THE ABOVE ADDRESS.

1. REPORT DATE *(DD-MM-YYYY)*	2. REPORT TYPE	3. DATES COVERED *(From - To)*
19-MAR-2010	Final Technical Report	01-DEC-2007 -- 31-OCT-2009

4. TITLE AND SUBTITLE

Computational Flow Analysis of Ultra High Pressure Firefighting Technology with Application to Long Range Nozzle Design

5a. CONTRACT NUMBER

FA4819-07-D-0001

5b. GRANT NUMBER

5c. PROGRAM ELEMENT NUMBER

63112F

6. AUTHOR(S)

Menchini, Christopher P.

5d. PROJECT NUMBER

4918

5e. TASK NUMBER

D2

5f. WORK UNIT NUMBER

Q130D8A3

7. PERFORMING ORGANIZATION NAME(S) AND ADDRESS(ES)

Applied Research Associates
P.O. Box 40128
Tyndall Air Force Base, FL 32403

8. PERFORMING ORGANIZATION REPORT NUMBER

9. SPONSORING/MONITORING AGENCY NAME(S) AND ADDRESS(ES)

Air Force Research Laboratory
Materials and Manufacturing Directorate
Airbase Technologies Division
139 Barnes Drive, Suite 2
Tyndall Air Force Base, FL 32403-5323

10. SPONSOR/MONITOR'S ACRONYM(S)

AFRL/RXQD

11. SPONSOR/MONITOR'S REPORT NUMBER(S)

AFRL-RX-TY-TR-2010-0038

12. DISTRIBUTION/AVAILABILITY STATEMENT

Distribution Statement A: Approved for public release; distribution unlimited.

13. SUPPLEMENTARY NOTES

Ref AFRL/RXQ Public Affairs Case # 10-100. Document contains color images.

14. ABSTRACT

Although aqueous fire fighting agent compositions have undergone considerable evolution in recent decades, agent stream optimization has lagged behind in development. A Computational Fluid Dynamic (CFD) modeling study analyzes Ultra High Pressure (UHP) jet stream characteristics as a function of nozzle flow conditions and fluid composition. A CFD sub-model analysis is also conducted to determine sensitivity to certain modeled assumptions. In addition, a steady co-flow augmented nozzle concept is analyzed to demonstrate nozzle enhancements to prolong jet reach. Experimental Laser Doppler Velocimetry (LDV) and Phase Doppler Particle Analysis (PDPA) field sampling provide computational boundary conditions and general observed flow characteristics where applicable. Results show flow factors that increase jet Reynolds and Weber number also increase jet reach. Multiphase, turbulent, and non-uniform droplet dynamic CFD sub-models affect solutions, but typically as a higher order effect. Steady co-flow nozzle results depict a negligible effect on extending jet reach. Further experimental validation data and CFD model development is required to create a dependable agent application optimization tool for the fire research community.

15. SUBJECT TERMS

ultra high pressure (UHP), throw distance, nozzle, turbulent fluctuations, polymer modifiers, co-flow air stream air flows, spiral 2 development, low velocity, extinguishing capability

16. SECURITY CLASSIFICATION OF:			17. LIMITATION OF ABSTRACT	18. NUMBER OF PAGES	19a. NAME OF RESPONSIBLE PERSON
a. REPORT	b. ABSTRACT	c. THIS PAGE			R. Craig Mellerski
U	U	U	UU	61	19b. TELEPHONE NUMBER *(Include area code)*

Reset

Standard Form 298 (Rev. 8/98)
Prescribed by ANSI Std. Z39.18

TABLE OF CONTENTS

LIST OF FIGURES

LIST OF TABLES

1.0 SUMMARY

A computational fluid dynamic (CFD) parametric study was conducted on Ultra High Pressure (UHP) agent application firefighting technology to study how variation in nozzle flow condition and fluid properties affect overall jet stream performance.

Nozzle discharge pressure, turbulence intensity, droplet size, and flow rate were flow conditions analyzed, and fluid density, viscosity, and surface tension were fluid properties analyzed. The output parameters that were reported included agent total pressure, velocity magnitude, turbulence intensity, phase fraction, turbulent kinetic energy, and turbulent energy dissipation rate, with droplet size effects where applicable. A CFD sub-model study was also performed to observe how physical modeling assumptions affect overall results. Multiphase, turbulence, droplet distribution interaction, and droplet drag law sub-models were examined. In addition, a steady co-flow nozzle concept was studied to determine if near field UHP jet shear layer augmentation methods can prolong UHP jet stream reach.

To support modeling efforts, experimental laser Doppler velocimetry (LDV) and phase Doppler particle analysis (PDPA) measurements were sampled on two similar low flow rate (38 and 53 l/min) UHP platforms. Field sampling in various jet flow regimes was conducted to test the applicable data acquisition limitations of both systems. Near field nozzle exit velocities and droplet size distributions were extracted to confirm CFD flow boundary condition settings. Both LDV and PDPA systems successfully recorded conclusive data throughout the physical range of the jet. In addition, field sampled data corroborated model results where applicable.

The CFD parametric study showed that an increase in UHP jet Reynolds number and Weber number extend jet reach. It also concluded that multiphase model implementation requires further investigation as each derivative was flow regime specific. Isotropic turbulence models also appear applicable for high Reynolds number flows which were representative of UHP operating regimes. Droplet interaction models affect jet flow field characteristics, but global effects were considered high order with a reduced return on computational investment. The steady co-flow nozzle analyzed to examine potential UHP stream reach extension effects returned poor performance results showing near negligible changes in jet characteristics. Alternative nozzle augmentation should be considered, possibly taking into account dynamic conditioning of the jet core shear layer.

Although several physical as well as computational conditions were examined, more work is needed to address recognized gaps in model fidelity, in addition to examining CFD techniques to resolve both agent application and fire suppression interaction. Further, a rigorous experimental analysis is needed to provide further insight into observed UHP jet dynamics, as well as better validation support for CFD model results and design tool development.

2.0 INTRODUCTION

2.1. Background

Ultra high pressure (UHP) agent application firefighting technology has seen steady development with regard to host vehicle and delivery system improvements including upgraded pump designs and enhanced control. UHP has become a premiere aircraft rescue firefighting (ARFF) technology, with suppression times approximately 25% lower and agent requirements 67% less than traditional hydrocarbon pool fire suppression methods [1]. For specific details on the evolution of UHP firefighting, refer to the Air Force Research Laboratory (AFRL) technical report detailing the design and development of a prototype UHP P-19 which includes an historical perspective [2].

A collection of field test data from UHP platforms was gathered in Figure 1 relating stream (jet) range to nozzle exit volumetric flow rate.

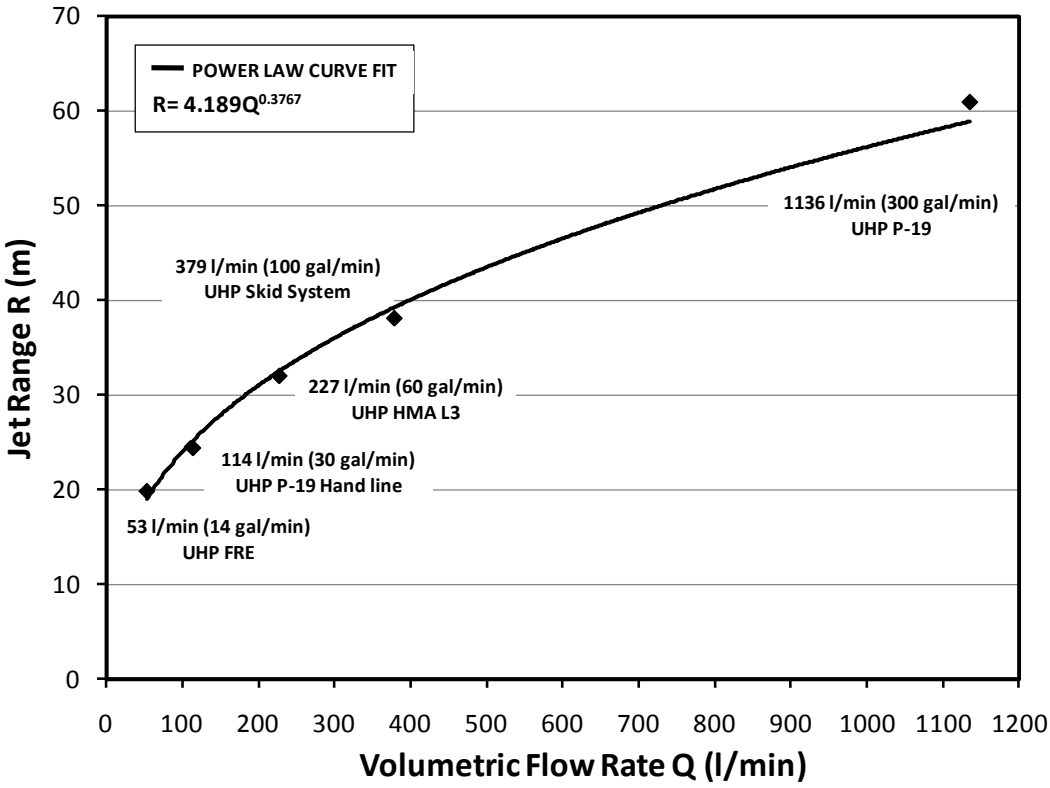

Figure 1. UHP Stream Range as a Function of Agent Flow Rate

All agent compositions were 6% aqueous film-forming foam (AFFF) by volume mixed with water, and jet range measurements were reported as defined by NFPA 412 [3]. 6% AFFF refers to 3% AFFF mixed at double the standard concentration. A power law was used to fit the data. It should be noted that nozzle types and profiles represented in Figure 1 were not consistent due to design evolution over time coupled with unique customer requirements specific to each platform. It also represents a mixture of both long-term AFRL/RXQD research efforts and commercially

transitioned platforms designed to meet rapid United States Air Force (USAF) deployment needs. These factors result in inconsistent dynamic similarity among platforms with jet Reynolds numbers (Re) spanning an approximate order of magnitude ($10^5 – 10^6$). In those Re regimes, jet flow was fully turbulent. In addition, as agent flow rates change, jet momentum changes corresponding to non-linear dynamic pressure effects causing further self-similar divergence. Because of this developmental path, UHP jet operating parameters have not been rigidly set, leading to a de facto definition of UHP nozzle exit pressures that range from approximately 60 to 100 bar (900 – 1500 lb/in^2).

With focus on upstream delivery system innovation, UHP nozzle design and understanding of agent transport from nozzle exit to the flame front has not been fully investigated. Several researchers have examined turbulent liquid jets exiting into ambient air, but little work has been conducted in the practical UHP firefighting regime tailored for higher flow rate / higher pressure applications. Kalberer and Grosskopf conducted experimental droplet diameter measurements on small-scale UHP water spray systems (3.9 – 23.3 l/min). They report a 50 – 120 μm (micron) average exit droplet diameter spanning a 120 – 250 m/s range corresponding to an exit pressure of 50 – 215 bar, demonstrating droplet diameters scale inversely proportional to nozzle exit velocities and pressures [4].

Theobald analyzed the stability of full-scale firefighting water jets measuring their range, dispersion, and trajectory for a variety of nozzle types. Although Theobald's study focused on relatively low nozzle exit pressures compared to UHP, it was concluded that maximum trajectory height was due primarily to pressure and secondarily to nozzle profile and size. It was also determined that concave nozzles with high near exit curvature provide the best all around jet performance in terms of range, stability, and ground pattern distribution over straight-sided nozzle profiles [5]. McCarthy and Molloy prefaced Theobald's work showing fully-developed flow exiting the nozzle has a first order effect on the exit velocity profile and in turn drives optimal jet surface and shape. Fully developed internal flows were typically characterized by nozzle length to diameter (L/D) ratios of 40 or greater for turbulent fields [6].

Husted, Petersson, Lund, and Holmstedt investigated fine water mist systems for interior fire suppression comparing and contrasting particle image velocimetry (PIV) and phase Doppler particle analysis (PDPA) measurement techniques for two nozzle types. After gathering jet water droplet velocities and diameter distributions, they concluded that both methods adequately characterize the sprays effectively, but both methods experience lower signal-to-noise ratios in the near nozzle exit regime due to heightened liquid jet core density [7]. Both Kalberer and Husted witnessed that an increase in jet flow rate increases momentum and furthers jet reach. However, it was also observed that higher velocities enhance liquid jet core breakdown increasing agent surface area, ultimately causing increased aerodynamic drag [4,7].

Yoon, Kim, and Hewson conducted a parametric study of coalescing and evaporating turbulent jet sprays using a modeled probability density function (PDF) approach to characterize initial nozzle exit conditions [8]. Although downstream droplet distribution profiles were comparable to experimental results, predicted results were highly dependent upon model constants derived from empirical results or from liquid core computations referenced by an earlier work of Yoon [9] as well as Park, Yoon, and Heister [10]. In addition, Yoon observed larger droplets dispersed

radically outward by the initial spray cone angle whereas smaller droplets converged inward due to aerodynamic drag interaction with the surrounding air [8].

There were numerous studies similar to Yoon's work [8] that focus on interior sprinkler system applications with low flow rates, high pressures, wide spray angles, and small, well dispersed droplet sizes providing wide area coverage from a static location. By contrast, traditional ARFF agent application techniques were lower pressure, higher flow rate, narrower more continuous jets optimized for mobilized aircraft fire suppression. UHP combines these approaches by energizing the traditional ARFF stream into a more turbulent jet. This results in increased agent break-up causing dispersed finer droplets to form at jet extremities, while still maintaining a semi-continuous liquid core that grows more pronounced as flow rate increases. Figure 2 qualitatively compares each jet shape and droplet range make-up.

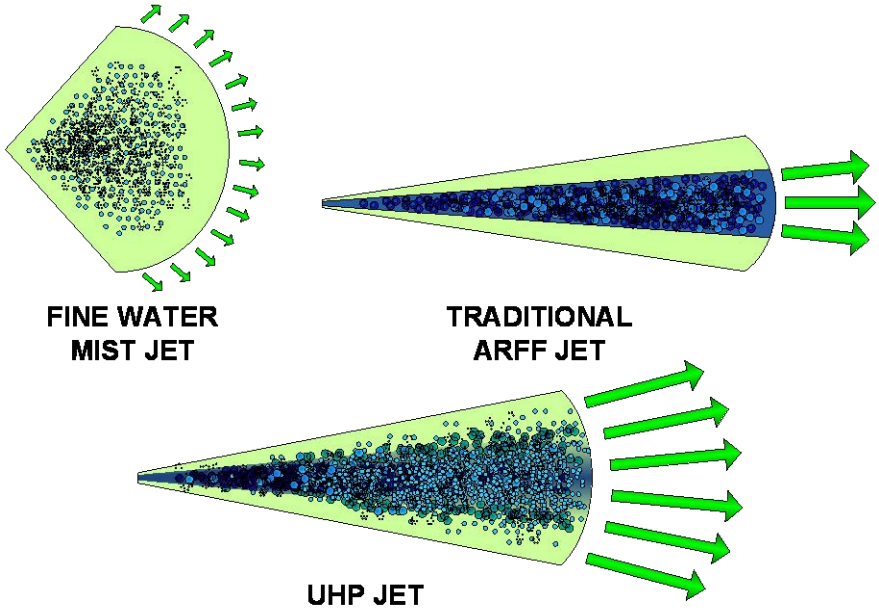

Figure 2. Qualitative Comparison of Firefighting Agent Application Jet Dynamics

2.2. Scope

The purpose of this report was to analyze multiple flow parameters to describe UHP jet characteristics with the aid of computational fluid dynamics (CFD). Extrinsic nozzle discharge parameters turbulence, droplet size, flow rate, and pressure were varied using homogeneous liquid water with constant properties as the agent medium. Intrinsic flow properties density, dynamic viscosity, and surface tension with air were then varied to observe agent composition effects. A CFD sub-model analysis including an array of multiphase, turbulence, droplet distribution interaction, and drag law descriptions were also examined to determine sensitivity to physical modeling assumptions. This work did not cover non-Newtonian viscosity effects exhibited by additives such as AFFF which causes emulsified foam to develop during the agent transport process. To further simplify the study, mass transfer between phases was neglected.

Temperature was also held constant providing ambient isothermal conditions throughout the flow field.

Experimental LDV and PDPA field sampled data was used for CFD boundary conditions, presented first to introduce observed jet physics. CFD model development was then discussed summarizing each sub-model, physical assumptions made, and spatial mesh domain extents required to describe the entire flow field. A simplified 53 l/min (14 gal/min) UHP First Response Expeditionary (FRE) vehicle nozzle was used for most of the analysis representing the baseline flow rate condition. Extensions to a 379 l/min (100 gal/min) and 1136 l/min (300 gal/min) geometrically similar but scaled up nozzle and domain were used to examine flow rate effects. In addition, a conceptual co-flow nozzle was studied to demonstrate model applicability to augmented nozzle design and optimization.

2.3. Terminology

This report assumes the reader has familiarity with basic terms and concepts commonly used in the experimental and computational fluid mechanics arena. For further details on any particular topic, the reader is referred to the associated reference. All units and physical dimensions were presented in SI units, with equivalent English system units reported for helpful interpretation.

3.0 EXPERIMENTAL LDV/PDPA FIELD SAMPLING

3.1. Experimental Overview

Laser Doppler Velocimetry (LDV) and Phase Doppler Particle Analysis (PDPA) field sampling measurements were conducted as part of a feasibility study to determine if accurate droplet velocity, turbulent statistics, and size measurements within a 6% AFFF UHP jet could be gathered. LDV is a non-intrusive measurement technique used on seeded particulate (or droplet) flow fields to measure velocity magnitude and direction principally based upon the Doppler frequency shift of scattered laser light [11]. PDPA, similar in operating principle to LDV, goes a step further using the phase shift from multiple photo detectors to calculate particle diameters [12].

Although there have been several LDV/PDPA analyses done on water sprays, sparse data was available on surfactant-based water jets – especially in UHP operating regimes. Because both data acquisition (DAQ) events were brief field sampling exercises, the data presented should be acknowledged as representative of the measured flow regimes, but not interpreted as a rigorous description of the entire flow field.

A 53 l/min (14 gal/min) UHP First Response Expeditionary (FRE) vehicle platform and 38 l/min (10 gal/min) UHP Rosenbauer skid unit were chosen to represent practical ARFF flow rates with significant stream density near the nozzle exit, but not too high as to create significant DAQ challenges. With a maximum reach on the order of 20 m, the UHP FRE jet was small enough to accommodate indoor test conditions shrouded from outside wind effects. The FRE can store 197 liters (52 gallons) of water as well as a 9 liter (5 gallon) foam tank providing about 3.7 minutes of continuous fire suppression. The UHP fire suppression power plant was independent of the

FRE vehicular drive train. Figure 3 depicts the FRE vehicle and Figure 4 depicts the UHP FRE nozzle details including a cross-sectional view of the nozzle geometry highlighting the interior flow path. The nozzle exit diameter was approximately 3.5 mm, and the internal profile mimics an orifice plate – style design with the fog to straight stream transition controlled by rotating the forward hand grip. The UHP Rosenbauer skid system was made up of similar hardware.

Since this study's ultimate goal was to examine methods to extend jet reach, the FRE straight stream configuration was the only pattern experimentally investigated with either LDV/PDPA system as the fog pattern creates a more dispersed, shortened jet pattern.

Figure 3. The 53 l/min (14 gal/min) UHP FRE Vehicle

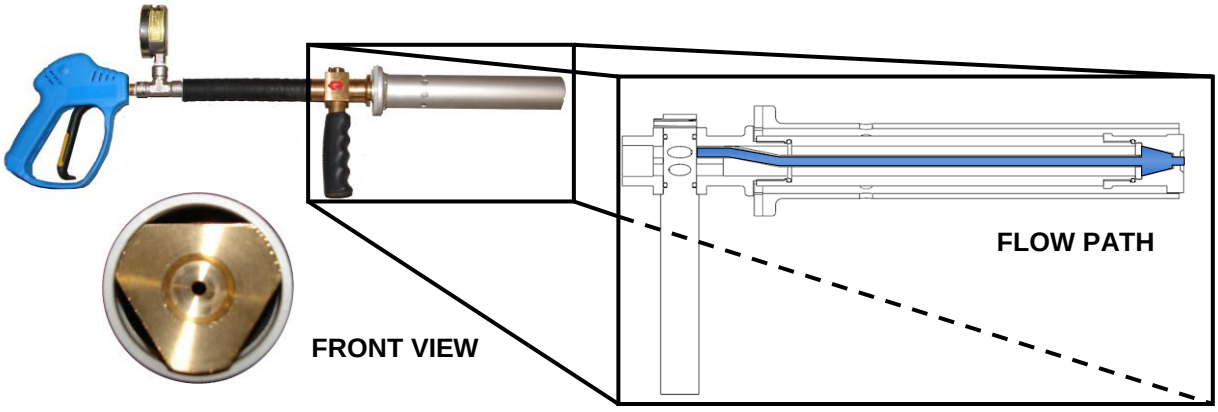

Figure 4. The 53 l/min (14 gal/min) UHP FRE Nozzle Details and Internal Flow Path Depiction

3.2. Experimental Data Acquisition Equipment

A one-dimensional (1-D) LDV system was provided by Dantec Dynamics to represent a compact, relatively inexpensive measurement solution capable of capturing instantaneous velocity measurements and gather turbulent statistics. A two-dimensional (2-D) PDPA system was provided by TSI, Inc. to represent a more detailed but also more costly analysis capable of measuring instantaneous velocity, turbulence statistics, as well as particle droplet diameters in multi-dimensional space. Figure 5 and Figure 6 depict the 1-D LDV system and major 2-D PDPA system components, respectively. For information regarding the technical DAQ process for both the LDV and PDPA system, the reader was referred to the technical guides provided by both manufacturers, respectively [11,12].

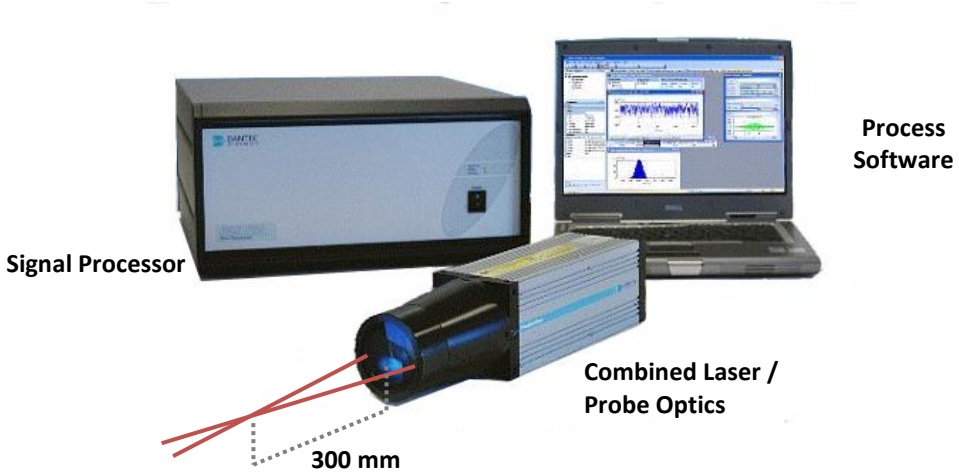

Figure 5. 1-D LDV System [11]

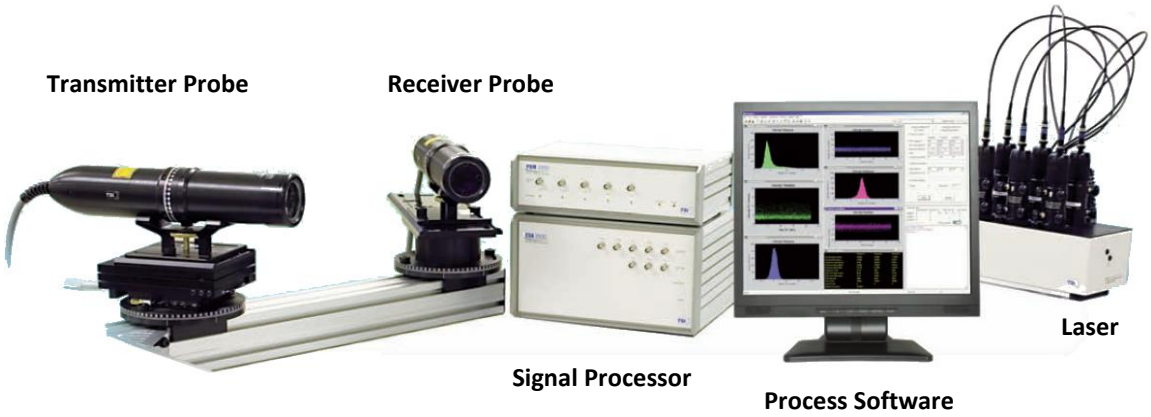

Figure 6. 2-D PDPA System [12]

3.3. Experimental Data Acquisition Process

LDV sampling was conducted on-site with the UHP FRE at the Tyndall AFB, FL AFRL Test Range I inside of the AFRL/RXQD fire garage where water and foam drainage were easily managed through pre-configured pipes. All software and post processing equipment was stationed away from the UHP jet spray, with probe optics positioned in the jet near field and shrouded to avoid contamination. A backboard was positioned to aid laser alignment. PDPA measurements were accomplished at the PDPA manufacturer headquarters in Shoreview, MN due to locality near the FRE equipment manufacturer. These measurements were conducted outside because of limited indoor space.

Both DAQ systems relied on extremely fast signal processers to interpret data being recorded on the order of 50,000 samples per second, primarily to account for UHP nozzle exit velocities (approximately 100 m/s) and to accurately capture small-scale turbulent fluctuations. Figure 7 shows the complete LDV set-up with Figure 8 showing the DAQ process. A similar set-up was created off-site for the PDPA system and the UHP Rosenbauer skid unit, with Figure 9 showing the PDPA DAQ process relative to the UHP jet spray.

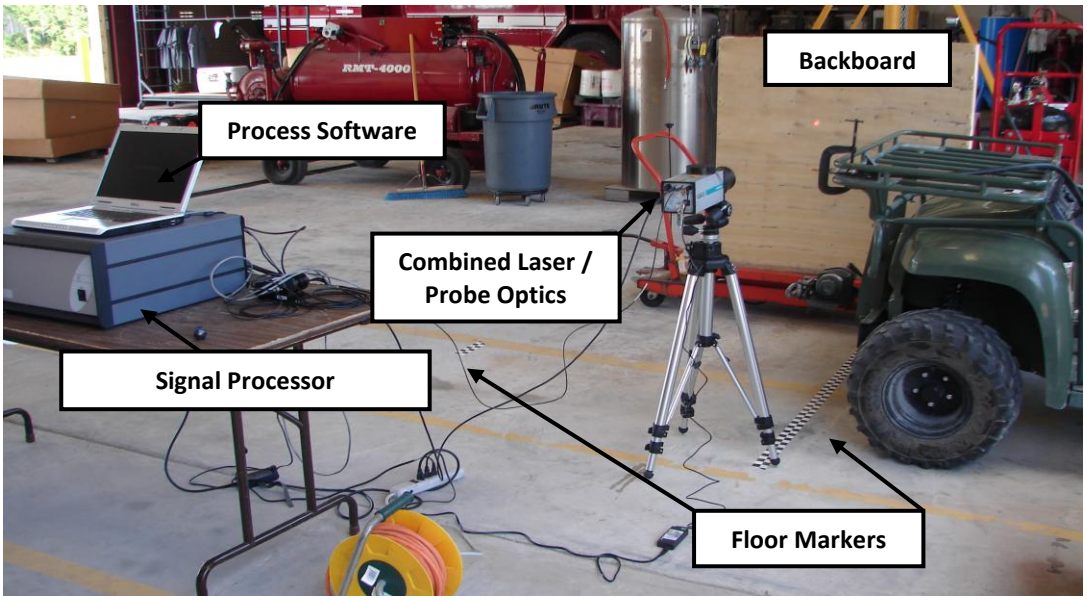

Figure 7. 1-D LDV Field Sampling Overview

(a) (b)

Figure 8. (a) The 6% AFFF UHP FRE Nozzle Accompanied by the 1-D LDV System (b) UHP FRE 1-D LDV System in Action Recording Instantaneous Velocities for the Water Only UHP FRE Spray

(a) (b)

Figure 9. (a) The 2-D PDPA System Measuring the UHP Rosenbauer Water Spray (b) The 2-D PDPA Laser and Multi-channel Signal Processor

Data samples were taken at jet centerline point locations in the near field of the nozzle exit where the liquid core was most dense and nearly continuous, points in the far field where droplet densities were low and fully dispersed, as well as intermediary locations between both extreme regimes. In addition, a 2-D velocity profile was recorded approximately 0.5 meters downstream of the nozzle exit. Data was also gathered with both 6% AFFF and water only sprays to compare measured trends.

3.4. Analysis of Experimental Data

Figure 10, Figure 11 and Figure 12 depict data collected for both the 1-D LDV and 2-D PDPA field sampling exercises at a point approximately 2.5 cm downstream of the UHP FRE nozzle with a combination of water only and 6% AFFF agent compositions. Nozzle near field observations showed little difference in UHP jet characteristics between water only and 6% AFFF compositions. This zone was selected for presentation due to the initial conditions the data

suggested for implementation into the computational flow model. The average velocity for this measurement was 101.3 m/s, an RMS velocity of 10.9 m/s leading to an average turbulence intensity of about 10% recorded by the 1-D LDV and reflected in Figure 10. Approximately 200,000 samples were recorded for each near field data point with quasi-steady state conditions observed for the majority of the near field jet core. The 2-D PDPA measured a droplet distribution of both water only and 6% AFFF spanning three orders of magnitudes with recordings ranging from 1 to 160 μm, with the majority of diameters falling between 5 and 25 μm as reported by Figure 11. The PDPA droplet diameter was reported over 50 bins or particle group families, discretized by the DAQ software.

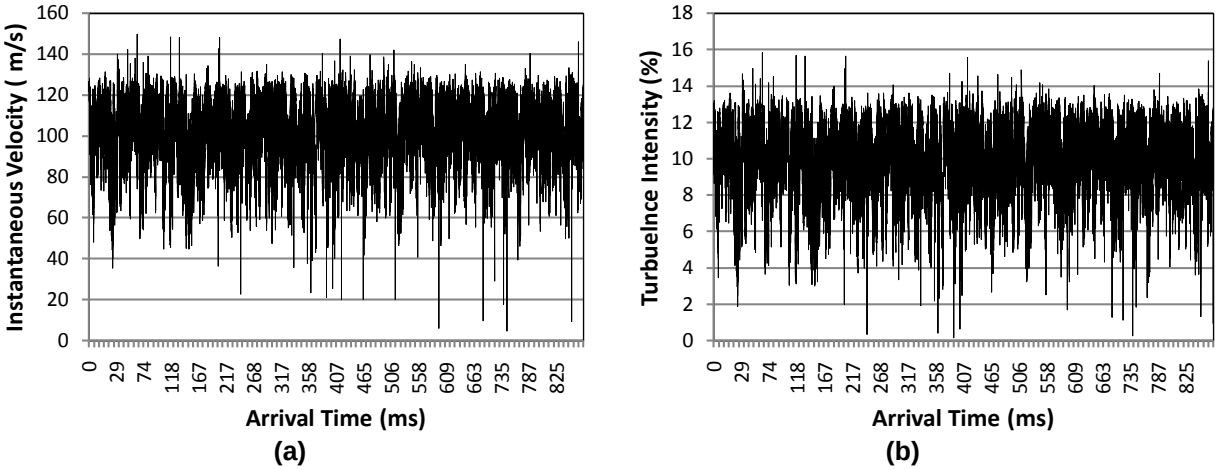

Figure 10. 1-D LDV (a) Instantaneous Velocity and (b) Turbulence Intensity Raw Data Output 2.5 cm Downstream from the 53 l/min (14 gal/min) UHP FRE Nozzle Exit

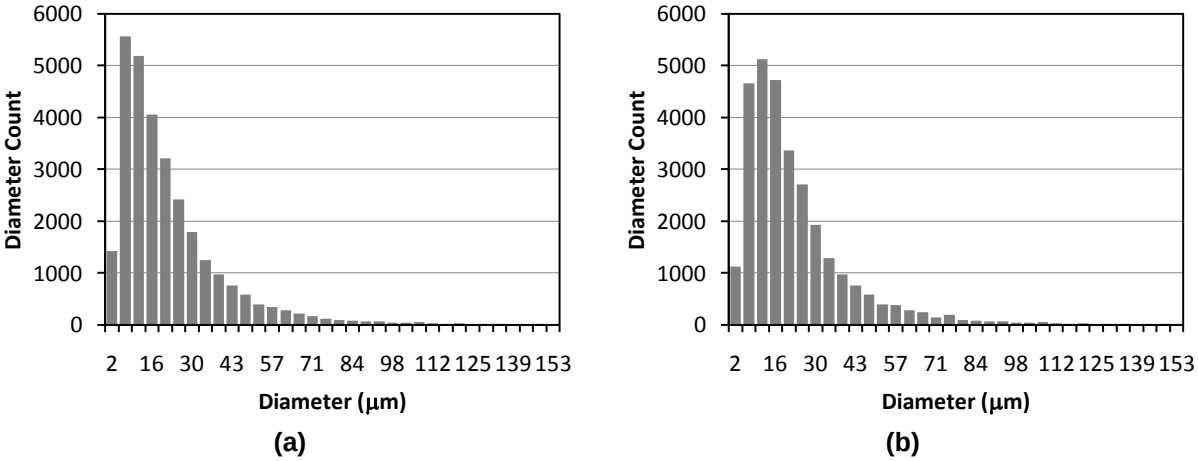

Figure 11. 2-D PDPA (a) Water Droplet Diameter Distribution and (b) 6% AFFF Droplet Diameter Distribution 2.5 cm Downstream from the 53 l/min (14 gal/min) UHP FRE Nozzle Exit

A mean velocity profile was recorded by the 1-D LDV taking data every millimeter over a 12 mm span covering the local width of the jet. With a 3.5 mm nozzle exit area, the jet spray expanded approximately 3.5 times over the 2.5 cm stream-wise distance. Figure 12 depicts these

results, both with water only and 6% AFFF compositions in approximately the same location downstream.

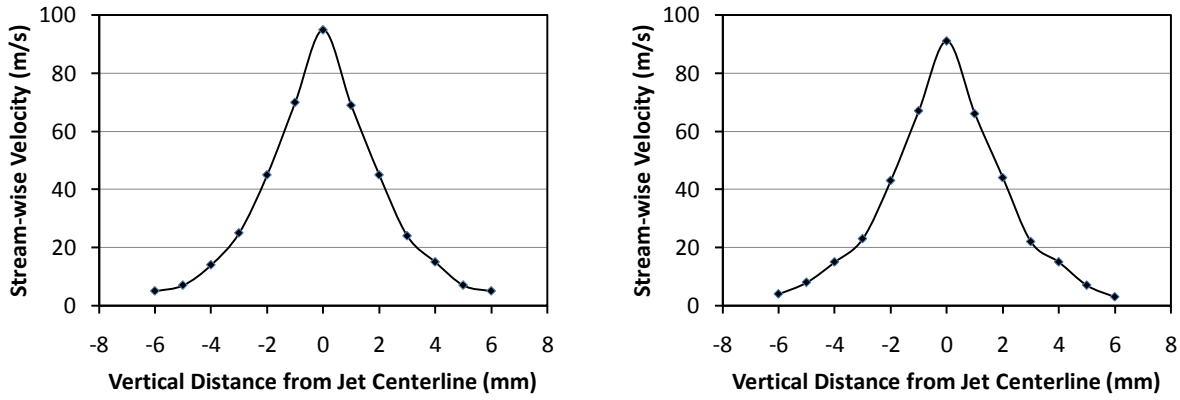

(a) **(b)**

Figure 12. 2-D PDPA (a) Water Only and (b) 6% AFFF Vertical Velocity Profile 2.5 cm Downstream from the 53 l/min (14 gal/min) UHP FRE Nozzle Exit

Data was collected further downstream with both measurement devices gathering similar results showing a non-linear drop-off in jet velocity reflective of basic fluid theory [13]. Real-time DAQ per point took approximately 3 to 5 seconds in areas near the nozzle exit where the jet core and particle density was most dense, and upwards of 20 to 30 seconds in the downstream very dispersed droplet regime where particle counts took relatively longer. Because a traverse system was unavailable to precisely locate the measurement location relative to the nozzle exit, combined point data reporting over entire jet lengths was neglected.

4.0 COMPUTATIONAL FLOW MODEL DEVELOPMENT

4.1. Background

Computational fluid dynamics (CFD) is a branch of continuum mechanics where the governing conservative fluid transport equations are solved simultaneously over a discretized spatial domain to provide solutions to physical fluid flow problems often impossible to solve analytically [14]. For this work, which investigates the solution of turbulent, multiphase free jets, no closed form analytical solution currently exists.

There were several CFD modeling methods available in ANSYS Fluent v12.1 capable of representing a wide array of observed UHP jet physics. Unfortunately, there was no practical modeling technique able to capture the universal details of an entire UHP jet from nozzle exit to flame front. This was due to the inherent complexity in modeling the transient liquid core break-up process. Several multiphase modeling strategies provide excellent approximations in specific jet regimes, spanning both Eulerian (continuum-based) and Lagrangian (discrete particle-based) concepts. The volume of fluid (VOF) method was a simplified derivative of the Eulerian model able to approximate the near nozzle liquid core break-up by explicitly resolving droplet shedding arising from jet instability with combined surface tension effects. Although transient VOF modeling comes closest to resolving first principle physics, spatial as well as temporal numerical resolution requirements became unmanageable spanning micron-sized droplets compared to tens of meters of jet reach. Although advanced mesh adaptation methods reduce computational overhead, this approach requires advanced resources beyond the scope of this study which focuses on rapid jet flow field solutions spanning a wide metric of conditions [15].

Discrete phase modeling (DPM) uses an Euler-Lagrange methodology by tracking particle trajectories through the fluid medium, in this case agent droplets through the ambient air. This strategy assumes an initial discrete droplet size distribution and velocity via an injection zone within the continuous Eulerian field, and can be solved coupled or uncoupled to it. By comparison DPM was computationally more efficient than VOF, but high resolution temporal and spatial scales must be accounted for similarly to resolve high frequency transient break-up details near the nozzle exit. Numerical stability was also less of an issue, but problems can arise in the near nozzle vicinity where the jet core maintains a near 100% liquid phase fraction. A significant limitation of DPM modeling was that the dispersed phase must maintain a volume fraction of 10% or less throughout the flow field. The dense discrete phase modeling (DDPM) method, a more strongly coupled Euler-Lagrange strategy, relaxes this limitation by tracking extra Eulerian transport equations to account for dispersed phase volumetric occupancy. DDPM was more challenging to implement due to stricter field coupling requiring added computational cost to solve extra conservation equations [15]. In addition, DPM was currently the only multiphase model compatible with the combustion models resident in ANSYS Fluent v12.1, the CFD solver in use for this study and concurrent AFRL/RXQD combustion modeling efforts.

4.2. Model Overview

The standard Eulerian model was the baseline multiphase model chosen for this analysis due to its efficient representation of the secondary (dispersed agent) phase coupled with reasonable

mesh requirements and adequate numerically stability. There was also no upper limitation on secondary phase volume fraction, favoring 100% to near 0% agent volume fraction transition from a continuous liquid core to a dispersed droplet flow field. With the addition of RANS turbulence modeling, stable steady-state solutions for the flow conditions of interest were achievable. Although high frequency turbulent jet break-up was not explicitly considered, essential physics was represented implicitly allowing modeled turbulent flow field fluctuations to provide appropriate feedback to the mean flow. Since the Eulerian model allows for customized dispersed phase interaction with respect to agent droplet size and general dynamics, population balance mechanisms were utilized to take droplet aggregation, break-up, and general redistribution into account. A structured 2-D axisymmetric geometric flow domain was used to reduce computational needs and expedite results. The following sections discuss the details of each CFD sub-model along with a description of the computational meshes employed to calculate results. For further information on all of the CFD modules discussed in this and subsequent sections, the reader is referred to the appropriate ANSYS Fluent v12.1 theory guides [15,16].

4.3. Multiphase Flow Modeling

The standard Eulerian multiphase model describing UHP jet physics was represented by a primary (continuous) and secondary (dispersed agent) phase, ambient air and homogenous water droplets, respectively, under the gas-droplet flow formulation assumption. The model uses a sophisticated Euler-Euler modeling approach defining a set of *n* – momentum and continuity equations for each phase. Water was treated as a constant property liquid, and air was treated as an incompressible ideal gas. Phase coupling was accomplished via pressure and phase exchange coefficients, where phase fraction must be specified at inlet and outlet boundaries. Mass transfer between phases was negligible due to assumed isothermal flow field conditions [15].

Within the dispersed phase, water droplets were defined as inert spherical particles under the influence of aerodynamic drag mostly governed by empirically derived relationships. Multiple drag laws were analyzed for this analysis, but the universal law was applied for the baseline condition providing the most sophisticated representation of droplet drag with a unique mathematical description for the Stoke's ($Re < 1$), viscous ($1 \leq Re \leq 1000$), and Newtonian flow regimes ($Re > 1000$). The universal drag law also had extensions to non-spherical particles for potential application to AFFF-based foam growth effects. Surface tension effects were accounted for in this model via the Rayleigh-Taylor instability wavelength function which was a component of the general drag law formulation. The Morsi-Alexander model was the most reliant upon empirical relations defined by an array of second order piece-wise polynomials governed by local discrete droplet Re regimes. The symmetric drag law defines the particle drag coefficient using a loose exponential curve fit for the viscous and sub-viscous regimes, which converges to a constant value as the flow re-enters the Newtonian regime. The symmetric drag law was the most numerically stable of all examined models recommended for flows where the secondary dispersed phase in one region of the domain becomes the primary continuous phase in another. The Schiller-Naumann drag law was similar in composition to the symmetric law and was the solver default. The only exception was that phase exchange coefficients were more simply defined relying on phases to maintain more consistent roles throughout the entire flow field [15].

The steady VOF model, a simpler derivative of the standard Eulerian model, was also considered in the CFD sub-model study to determine the sensitivity of model complexity versus variation in results. The VOF model, briefly described in Section 3.1, assumes a sharp interface between the primary and secondary phase with more limited mass transfer effects between the two [15].

4.4. Population Balance Modeling

Population balance (PB) modeling exclusively available in the standard Eulerian model was a supplemental module for capturing the effects variable droplet size and interaction play in shaping secondary phase dynamics. A droplet size distribution was initialized at the nozzle inlet. Based upon various predefined interaction mechanisms, droplets can nucleate, grow, disperse, aggregate, and break-up. Several PB sub-models accounting for all of these transactions were available, but only aggregation, break-up, and constant size redistribution were considered for this study involving pure water droplets. The discrete method was employed where droplets were divided into a finite number of families or bins based upon diameter. Each family was a separately tracked conservation equation favoring dispersed phases not spanning more than two to three orders of magnitude due to increasing computational requirements [16]. This numerical strategy was conducive to modeling a measured PDPA range covering approximately 1 to 160 μm near the UHP FRE nozzle exit. Seven bins were selected to discretize the droplet ranges present in the UHP jet. Table 1 tabulates the droplet diameter allocations at the nozzle exit boundary condition via volume fraction representative of the distribution measured by experimental PDPA field sampling.

Table 1. A Summary of Droplet Size Distribution

Bin No.	Volume Fraction (%)	Droplet Diameter (μm)
0	1	160
1	3	100
2	8	63
3	14	40
4	19	25
5	31	16
6	24	10

Droplet breakage frequency was carried out using the Luo model where smaller daughter particles were created based upon turbulent eddy-droplet interaction via a probability density function (PDF) approach. Droplet aggregation was accomplished with the Luo aggregation model using similar turbulent mixing principles where local shear magnitudes within the turbulent eddies govern the particle collision rate. These factors were driven by relating the local particle diameter with the corresponding turbulent spatial scale which ultimately dictates droplet aggregation behavior [16]. Droplet nucleation and growth were not considered as these two phenomena were typically associated with interphase mass transfer, assumed negligible due to insignificant condensation and evaporation via isothermal conditions. Population balance droplet interaction as it relates to the sub-modules selected for this study is illustrated in Figure 13.

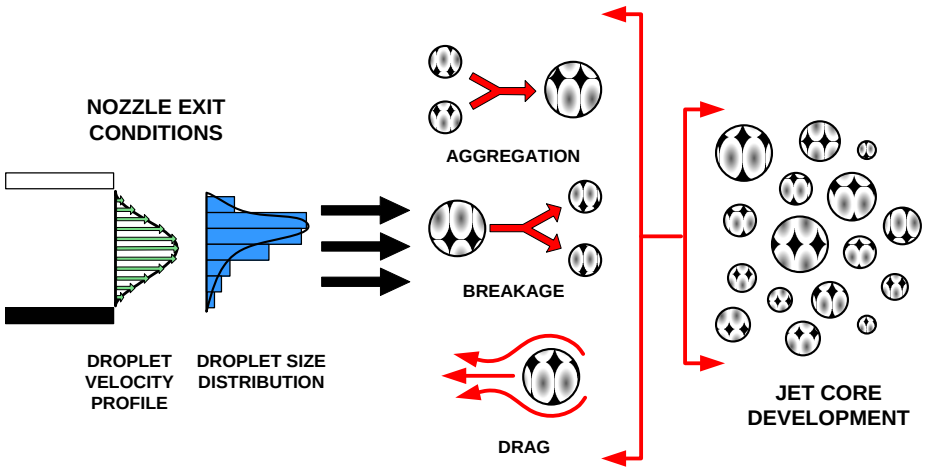

Figure 13. Population Balance Droplet Interaction

4.5. Turbulence Modeling

There were a variety of Reynolds averaged Navier-Stokes (RANS) based turbulence models available for use in conjunction with the standard Eulerian multiphase flow model. The two-equation k-ε model was selected due to its wide industrial application in accurately representing turbulent flows, requiring the additional solution of two extra equations accounting for the transport of turbulent kinetic energy (k) and its dissipation rate (ε). Because of their heuristic development, RANS models have applicable limitations and in general must be conditioned for the respective flow regime of interest. The Realizable k-ε model has been well-validated for turbulent round jet applications and was selected as the baseline turbulence model implementation. The baseline model was applied in mixture mode, tracking turbulence parameters for the unified multiphase flow field. This model was also examined on a per phase basis where turbulent quantities were tracked individually requiring two additional conservation equations. Alternative k-ε model derivatives analyzed for comparison were the standard and Renormalization Group (RNG) models, detailed in the ANSYS Fluent v12.1 Theory Guide [15]. Baseline turbulent boundary conditions were derived from LDV/PDPA field sampled data where nozzle exit turbulence intensity was approximately 10%, using a 0.0035 m turbulent length scale derived from the nozzle hydraulic diameter. Corresponding higher flow rates use their scaled nozzle diameters to define a respective turbulent length scale via hydraulic nozzle exit diameter.

4.6. Numerics

The CFD solution framework ranges from a 10 to 16 equation model based upon sub-model implementation. The pressure-based, multiphase coupled finite volume solver was used to solve the linearized system. Momentum, turbulence, energy, and population balance equations (when applicable) were solved second order upwind, with the QUICK scheme selected as the high order method for volume fraction transport. For more numerical details as well as model set-up details for the baseline model, the reader should refer to Appendix A: Baseline CFD Case Summary.

4.7. Physical Flow Domain

A 2-D axisymmetric mesh was used to represent the baseline UHP jet physical flow domain. Structured hexahedral cells were used due to their high aspect ratio efficiency in capturing strong nozzle near field gradients, but computationally conservative expandability in far-field quiescent regimes. The baseline (53 l/min or 14 gal/min) domain was made up of approximately 150,000 nodes, with a 3.5 mm straight bore nozzle representing a simplified version of the UHP FRE nozzle. The co-flow nozzle domain was identical in topology to the baseline edition with the exception of an added annulus about the liquid nozzle zone to inject highly energized air. The nozzle L/D ratio exceeds 40:1 for both the baseline and co-flow system, providing sufficient length to create fully-developed turbulent flow before exiting the nozzle. The nozzle inlets for both the liquid water and air were defined as a slug (uniform) inflow pressure inlet. A pressure inlet and outlet were combined to create far-field stagnation conditions, defined shape-wise to foster numerical stability due to ambient air entrainment. Figure 14 outlines the boundary conditions for the 2-D axisymmetric model. Figure 15 depicts the structured mesh topology showing near field differences between the baseline and co-flow domains.

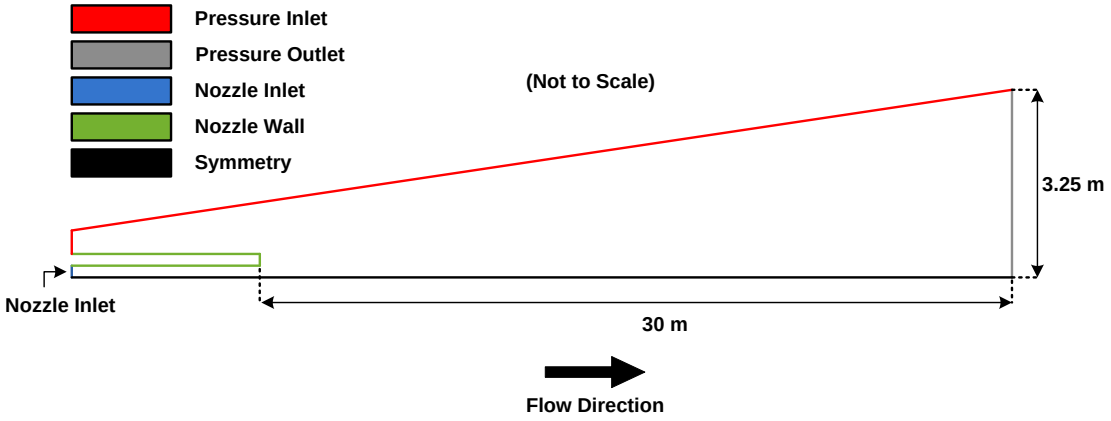

Figure 14. Boundary Condition Definition for the Baseline Balance Droplet Interaction

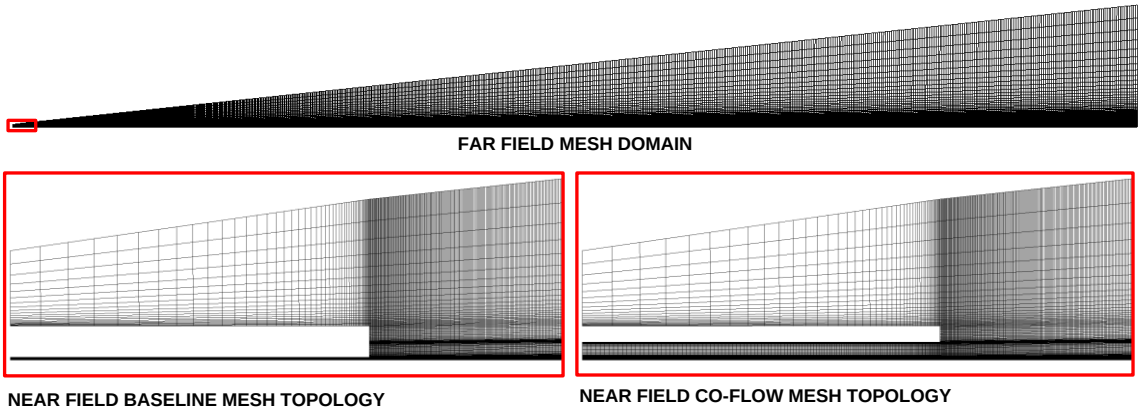

Figure 15. Geometric Mesh Depicting the Far-Field Domain as well as the Near Field Baseline and Co-Flow Topology

Table 2 outlines the three meshes employed to conduct the parametric nozzle flow rate study along with associated memory requirements and computational run times. The 379 l/min (100 gal/min) and 1135 l/min (300 gal/min) flow domain were similar in both shape and boundary condition prescription to the baseline 53 l/min domain, with an approximate 70 and 125 m extended domain, respectively, to account for higher agent flow rate ranges. All three grids reflect similar topologies depicted in Figure 14 and Figure 15. The 1136 l/min (300 gal/min) mesh required a distributed memory cluster due to its size (denoted by an asterisk), unlike the two lower flow rates which were executed on a single workstation computer.

Table 2. A Summary of Physical Flow Domains and Associated Computational Parameters

Flow Rate	Nodes	Cells	Memory (GB)	CPU Hrs
53 l/min (14 gal/min)	155K	153K	4.3	32
379 l/min (100 gal/min)	848K	844K	6.5	240
1136 l/min (300 gal/min)	2.57M	2.58M	14.4*	576

5.0 COMPUTATIONAL RESULTS

5.1. Parametric Study Overview

This study examined the effect differing nozzle conditions, agent fluid properties, and various modeling approximations have on global UHP jet flow field characteristics. Baseline parameters of 70 bar (1000 lb/in^2), 10% turbulence intensity, and constant 10 μm agent droplet size were selected as representative mid-range nozzle exit UHP jet conditions. Baseline fluid properties were selected to represent liquid water at standard sea level conditions. [13]. For a summary of baseline model conditions and set-up, the reader is referred to Appendix A: Baseline CFD Case Summary. For most of these analyses, two lower as well as two upper boundary values were evaluated with respect to the baseline condition, chosen within a practical range of applicability. Agent flow rate was examined at the baseline UHP FRE flow rate, as well as two higher application rates representative of past larger-scale demonstrator platforms. A select group of auxiliary modeling approaches were also assessed to examine how different physical modeling assumptions affect jet characteristics. In addition, an augmented co-flow nozzle concept was introduced to explore jet reach optimization methods.

Total pressure, velocity magnitude, turbulence intensity, phase fraction, turbulent kinetic energy, and turbulent energy dissipation rate were the main output parameters reported for each study. Certain parameters will be phase-based, whereas others will be mixture (water-air) based dictated by CFD sub-model selection. While variables like pressure, velocity, and phase fraction were factors easily understood and observed experimentally, turbulence quantities provided a sense of the jet's utilization of fluid energy – an important mechanism which helps define agent shape, transport characteristics, and distributed strength.

The majority of data is presented along the axisymmetric jet centerline, which generally captures the differences among applied parameters the best. In some instances, transverse rakes across the jet axis provide a supplemental perspective of interest. A select number of contour plots

highlighting the co-flow nozzle study provide flow visualization depicting flow structures indicative of most cases analyzed. Table 3, Table 4, and Table 5 summarize the nozzle condition, fluid property, and CFD sub-model studies, respectively. Baseline settings are highlighted in light gray.

Table 3. A Summary of Nozzle Condition Study Parameters

Nozzle Exit Parameter	Lowest	Lower	Baseline	Higher	Highest
Total Pressure (Bar)	40	55	70	85	100
Turbulence Intensity (%)	1	5	10	15	20
Droplet Size (μm)	1	5	10	100	200
Flow Rate (l/min)	--	--	53	379	1136

Table 4. A Summary of Fluid Property Study Parameters

Fluid Property	Lowest	Lower	Baseline	Higher	Highest
Density (kg/m^3)	500	750	1000	1250	1500
Dynamic Viscosity (kg/m-s)	1×10^{-4}	5×10^{-4}	1×10^{-3}	5×10^{-3}	1×10^{-2}
Surface Tension (N/m)	0.05	0.06	0.07	0.08	0.09

Table 5. A Summary of CFD Sub-Model Study Parameters

Model	Baseline	Auxiliary 1	Auxiliary 2	Auxiliary 3	Auxiliary 4
Multiphase	Eulerian	VOF	--	--	--
Turbulence	Realizable k-ε (Mixed)	Standard k-ε (Mixed)	RNG k-ε (Mixed)	Realizable k-ε (Per Phase)	--
Droplet Distribution Interaction	Constant Droplet Size	Aggregation / Breakage	None	Aggregation Only	Breakage Only
Droplet Drag Law	Universal	Symmetric	Morsi-Alexander	Schiller-Naumann	--

5.2. Nozzle Condition Study

A nozzle condition study was conducted whereby only extrinsic state changes to the fluid were analyzed leaving intrinsic material properties and CFD sub-models unchanged. The conditions chosen were typical of common experimentally controlled output parameters that typically enforce agent momentum and implied initial break-up state. Since Eulerian-based model assumptions were applied for this study, the secondary agent phase was considered a continuously homogeneous, although dispersed, medium.

Exit nozzle pressure settings were selected to span the entire observed UHP jet flow regime and beyond, intentionally conditioned to create 40, 55, 70, 85, and 100 bar (about 600 – 1500 lb/in^2). A 70 bar (1000 lb/in^2) nozzle exit pressure was selected for the baseline condition. The total pressure and velocity magnitude plots in Figure 16 illustrate that as pressure increases at the nozzle exit, a quasi-linear reduced return on increased momentum was experienced as

downstream distance from the nozzle increases. In addition, mean jet energy was proportionally converted into increasing turbulent kinetic energy and consequently dissipated at a higher rate as well. Downstream agent volume appears to be conserved along the jet centerline with a negligible effect on pressure variation.

Nozzle turbulence parameters were defined to create 1, 5, 10, 15, and 20% turbulence intensity exit conditions. 10% turbulence intensity was selected as the representative baseline condition. Turbulence intensity is a measure of the turbulent fluctuation magnitude relative to the magnitude of the mean flow. Figure 17 depicts that for all output parameters, a variation of turbulence intensity has a near negligible impact downstream of the nozzle.

Nozzle droplet size parameters were selected to create constant 1, 5, 10, 100, and 200 μm droplet diameter exit conditions. A 10 μm droplet size was selected as the representative baseline condition. Figure 18 illustrates that as droplet size increases, the corresponding output parameters increase in magnitude as well, with turbulent quantities showing the most substantial non-linear effects.

Flow rate exit conditions of Nozzle 53 l/min, 379 l/min, and 1136 l/min (14, 100, and 300 gal/min, respectively) were selected to analyze the role agent flow rate plays in defining UHP jet flow field characteristics. The 53 l/min (14 gal/min) flow rate was the representative baseline condition. The abscissa, or stream-wise x coordinate, has been non-dimensionalized to easily compare trends. Figure 19 depicts that nozzle flow rate has a significant, more complex impact on all output parameters, depicting increased momentum along the centerline as flow rate increases. Turbulent parameters see similar effects, but profile trends do not scale similarly. Volume fraction shows the most notable change in the nozzle flow condition study, showing significant increases in agent conservation along the jet centerline as flow rate was increased.

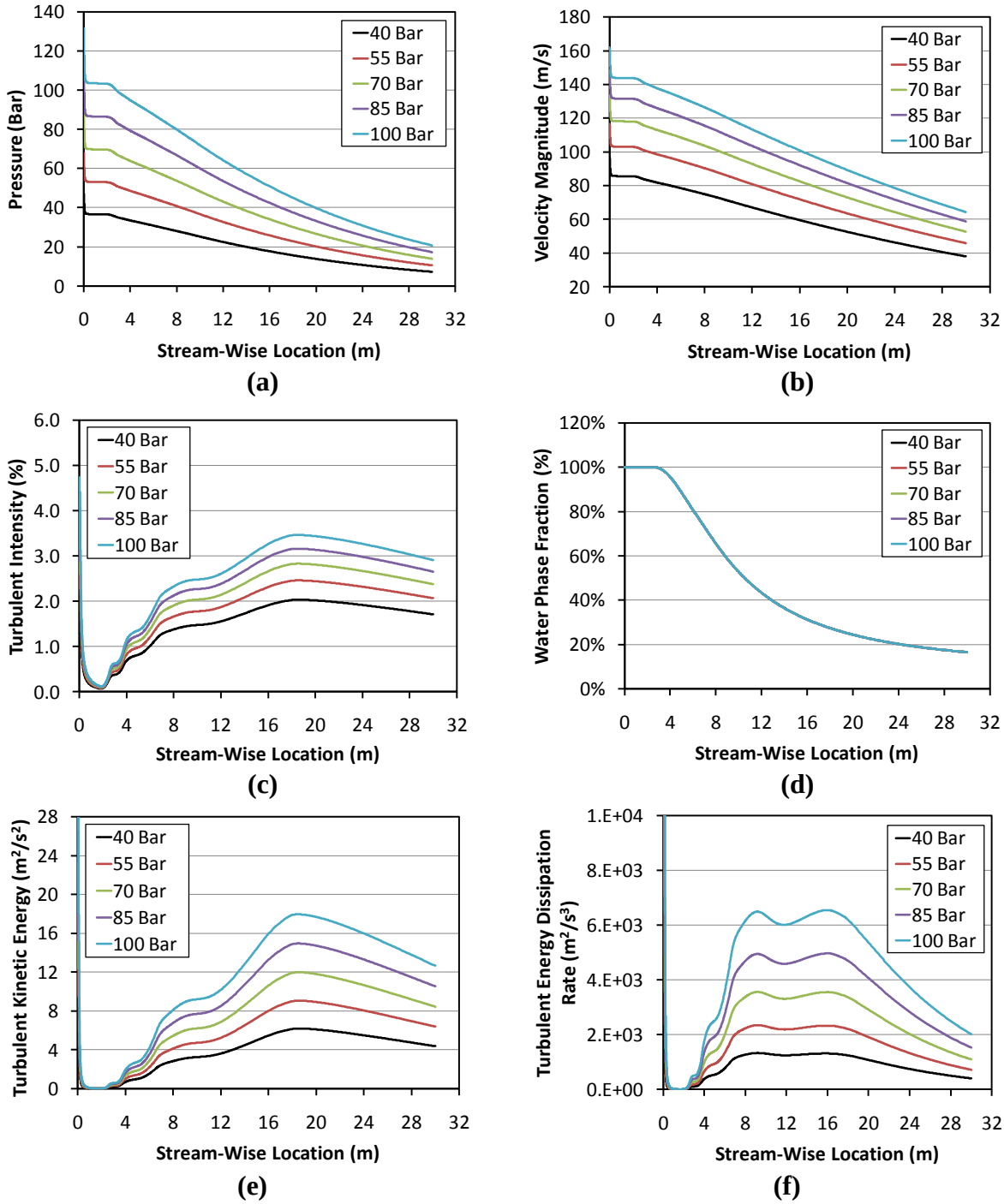

Figure 16. Nozzle Condition Study: Pressure Variation Along the Jet Centerline Showing (a) Pressure (b) Velocity Magnitude (c) Turbulent Intensity (d) Water Phase Fraction (e) Turbulent Energy Dissipation and (f) Turbulent Energy Dissipation Rate as a Function Of Stream-Wise Location from the Nozzle Exit

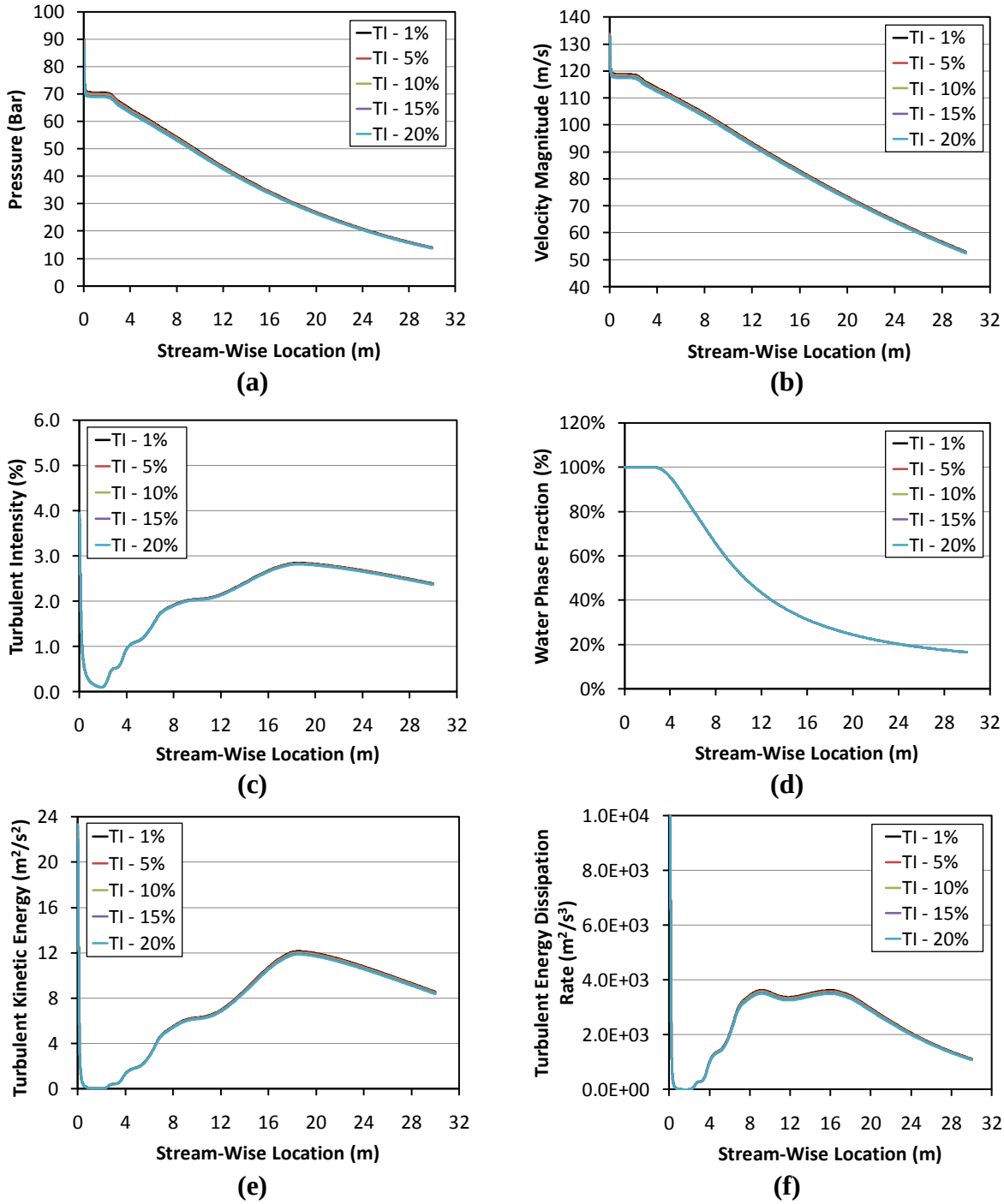

Figure 17. Nozzle Condition Study: Turbulence Intensity Variation Along the Jet Centerline Showing (a) Pressure (b) Velocity Magnitude (c) Turbulent Intensity (d) Water Phase Fraction (e) Turbulent Energy Dissipation and (f) Turbulent Energy Dissipation Rate as a Function of Stream-Wise Location from the Nozzle Exit

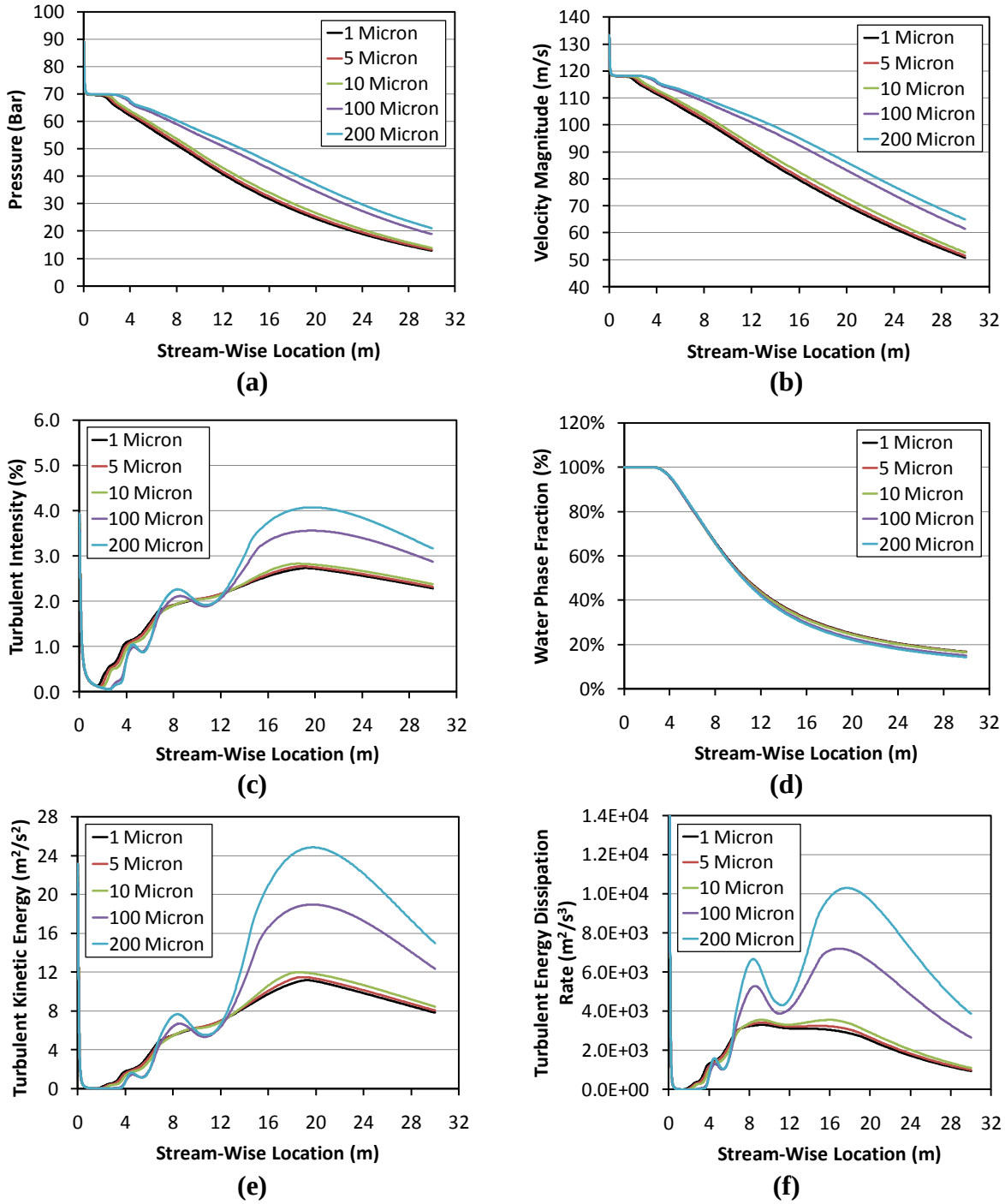

Figure 18. Nozzle Condition Study: Droplet Diameter Variation Along the Jet Centerline Showing (a) Pressure (b) Velocity Magnitude (c) Turbulent Intensity (d) Water Phase Fraction (e) Turbulent Energy Dissipation and (f) Turbulent Energy Dissipation Rate as a Function of Stream-Wise Location from the Nozzle Exit

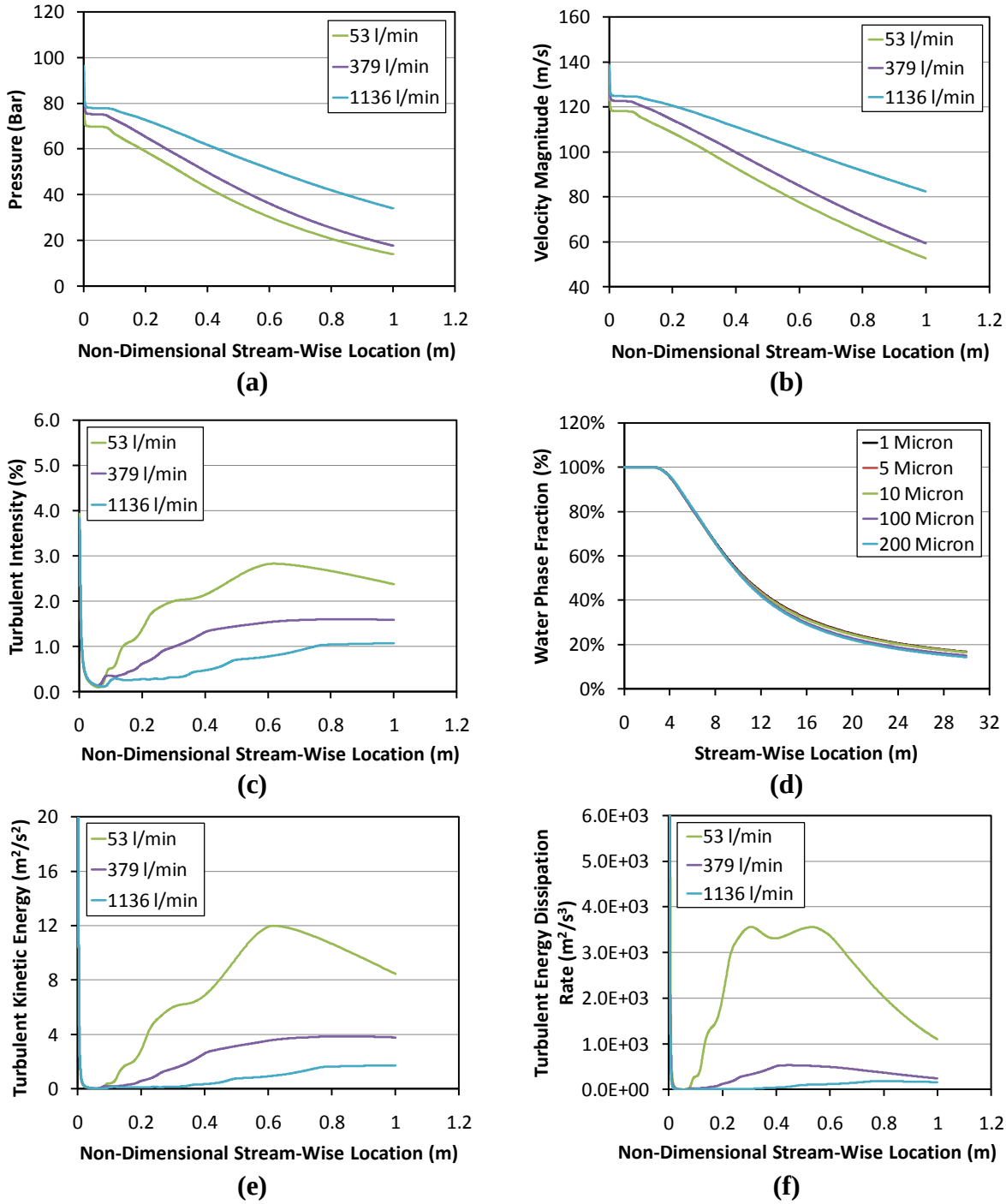

Figure 19. Nozzle Condition Study: Flow Rate Variation Along the Jet Centerline Showing (a) Pressure (b) Velocity Magnitude (c) Turbulent Intensity (d) Water Phase Fraction (e) Turbulent Energy Dissipation and (f) Turbulent Energy Dissipation Rate as a Function of Non-Dimensional Stream-Wise Location from the Nozzle Exit

5.3. Fluid Property Study

A fluid property study was conducted examining the intrinsic material properties of the agent while leaving nozzle exit flow conditions and CFD sub-model parameters constant. Factors such as agent material density, viscosity, and surface tension with the air were varied to interpret output flow field effects.

Fluid properties were defined to create 500, 750, 1000, 1250, and 1500 kg/m^3 agent densities to depict sensitivity to model conditions. 1000 kg/m^3 was the baseline condition representative of water at standard sea level conditions. Figure 20 illustrates that as fluid density increases, downstream total jet pressure increases. Velocity magnitudes follow similar trends, with decay rates decreasing as density was increased. Turbulence quantities also tend to decrease as density increases, depicting losses becoming less significant the more inertia the mean agent flow retains. In addition, agent volume along the centerline was weakly bled as agent density increases.

Agent dynamic viscosity was defined to generate 1×10^{-4}, 5×10^{-4}, 1×10^{-3}, 5×10^{-3}, and 1×10^{-2} kg/(m-s) agent compositions. Similar to baseline density selection, a 1×10^{-3} kg/(m-s) viscosity was selected as the baseline condition representative of water at standard sea level conditions. Figure 21 depicts that as fluid viscosity was decreased, output parameters globally increased, with water volume conservation along the jet centerline showing negligible transition. Inverse to fluid density changes, fluid viscosity output parameters trend in the opposite direction. This effect was explained by the dominant role the Reynolds number (Re) plays, a common non-dimensionless number used to relate a flow's inertial forces to viscous forces. It is often used as a measure of dynamic similarity between differing systems, defined as:

$$\mathrm{Re} = \frac{\rho V L}{\mu}$$

where ρ is the fluid density, V is the fluid velocity, L is the flow field characteristic length, and μ is the fluid dynamic viscosity [13]. Reynolds numbers were on the order of 10^5 to 10^6 for all flows analyzed in this study, corresponding to a fully turbulent jet flow regime.

Fluid properties were defined to produce 0.05, 0.06, 0.07, 0.08, and 0.09 N/m agent surface tension effects with air. These were practical quantities capable of altering the state of water by the use of additives. The 0.07 N/m standard surface tension of water with air was chosen for the baseline parameter. Figure 22 depicts a negligible global effect on altering surface tension by this degree. This observation was corroborated by the physical effect high (turbulent) Reynolds numbers have on correspondingly high (>> 1)Weber numbers (We), which is the measure of a flow's inertial forces relative to surface tension forces, defined by:

$$\mathrm{We} = \frac{\rho V^2 D}{\sigma}$$

where D is the droplet diameter and σ is agent surface tension [13]. Weber numbers were on the order of to 10^4 to 10^5 for all analyzed flow conditions, illustrating that inertial forces dominate surface tension effects for analyzed UHP jet flow regimes.

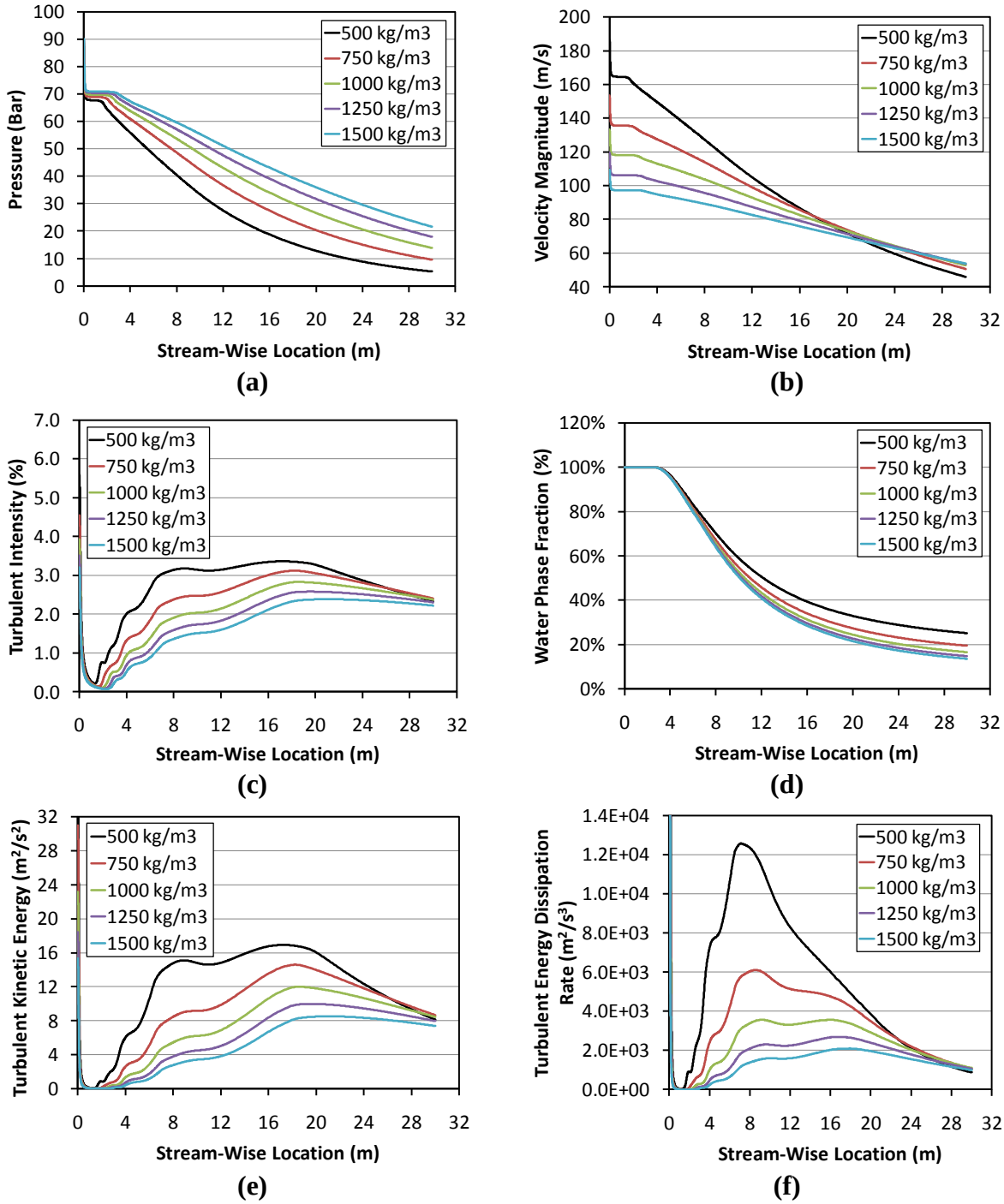

Figure 20. Fluid Property Study: Density Variation Along the Jet Centerline Showing (a) Pressure, (b) Velocity Magnitude (c) Turbulent Intensity (d) Water Phase Fraction (e) Turbulent Energy Dissipation and (f) Turbulent Energy Dissipation Rate as a Function of Stream-Wise Location from the Nozzle Exit

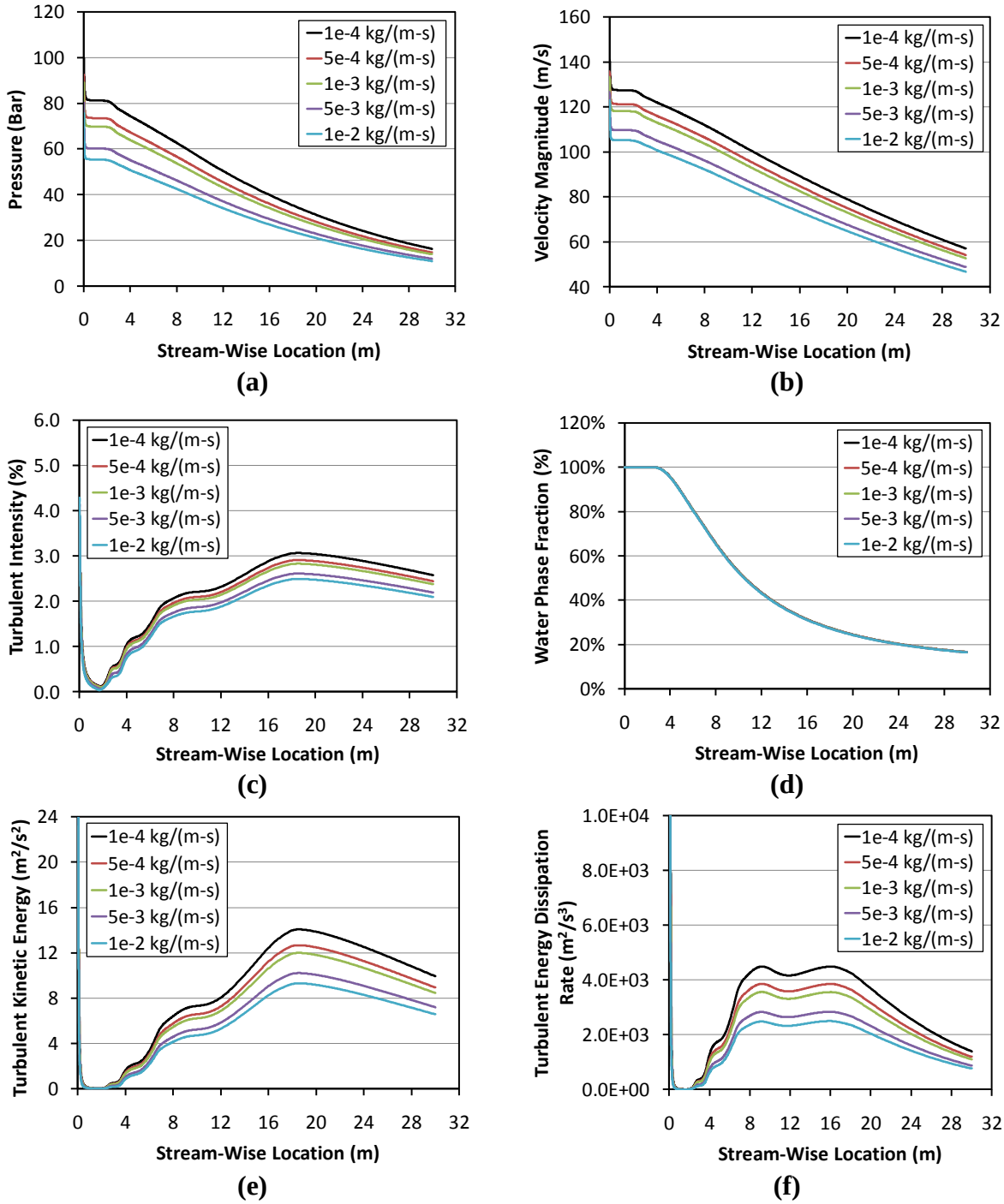

Figure 21. Fluid Property Study: Dynamic Viscosity Variation Along the Jet Centerline Showing (a) Pressure (b) Velocity Magnitude (c) Turbulent Intensity (d) Water Phase Fraction (e) Turbulent Energy Dissipation and (f) Turbulent Energy Dissipation Rate as a Function of Stream-Wise Location From The Nozzle Exit

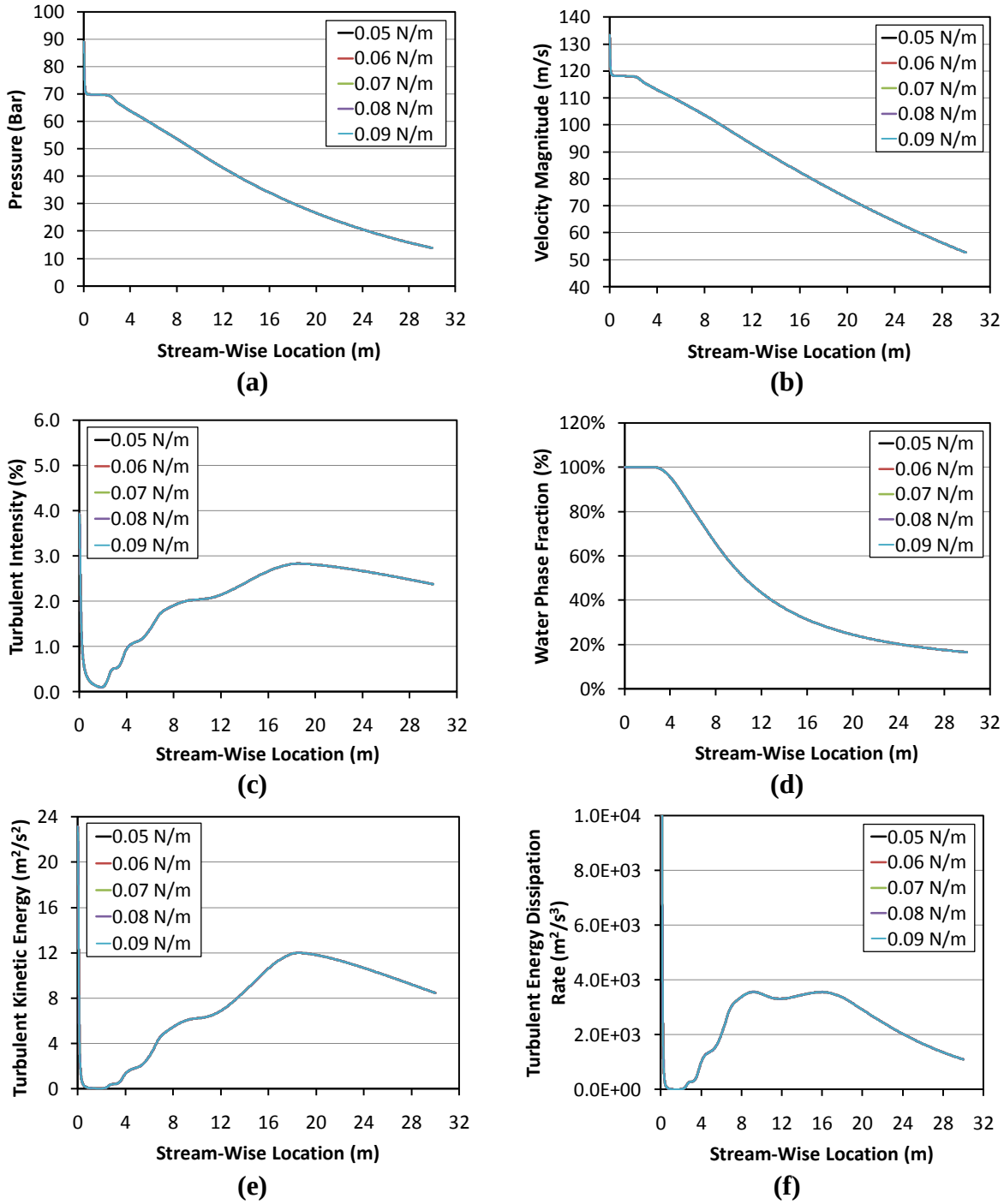

Figure 22. Fluid Property Study: Surface Tension Variation Along the Jet Centerline Showing (a) Pressure (b Velocity Magnitude (c) Turbulent Intensity (d) Water Phase Fraction (e) Turbulent Energy Dissipation and (f) Turbulent Energy Dissipation Rate as a Function of Stream-Wise Location From the Nozzle Exit

5.4. CFD Sub-Model Study

A CFD sub-model study was conducted examining the effect different model assumptions had on UHP jet flow field parameters of interest. Multiphase, turbulence, droplet interaction dynamics, and droplet drag law model variation were studied to interpret output sensitivity. Abbreviations used in plot legends that follow correspond to those shown in parentheses in the following paragraphs.

The standard Eulerian (Eulerian) and Volume of Fluid (VOF) models were examined with baseline nozzle exit conditions and fluid properties (See Table 3, Table 4 and Table 5). Figure 23 illustrates the results. Although velocity magnitude and turbulence quantities relay similar centerline jet behavior, the largest discrepancy was found via the flow field pressure with VOF depicting a significantly higher decay rate in comparison to the standard Eulerian model. This was indicative of the Eulerian dispersed phase assumption versus the more cohesive agent medium VOF represents mathematically. Agent volume fraction shows little divergence from one another.

Multiple variants of the two-equation k-ε turbulent RANS model were analyzed to provide insight on physical model assumptions versus change in output parameter. The Standard k-ε (Standard K-E), k-ε RNG (RNG K-E), and Realizable k-ε Mixture (Real K-E Mix) as well as k-ε per phase (Real K-E Phase) models were presented, with the realizable k-ε mixture model providing baseline conditions. Figure 24 depicts the results. The Real k-ε per phase model was unavailable for turbulence intensity (Figure 24c) reporting due to model reporting incompatibility. UHP flow field pressures and velocities show subtle differences, however trends and magnitude variation was generally weak. The standard k-ε model reports the strongest conversion of mean flow energy to dissipated turbulent losses, with the k-ε per phase version of the model bounding the opposite extreme. The baseline turbulence model falls midway through both, with water volume fraction variation depicting a weak function of all examined turbulence models.

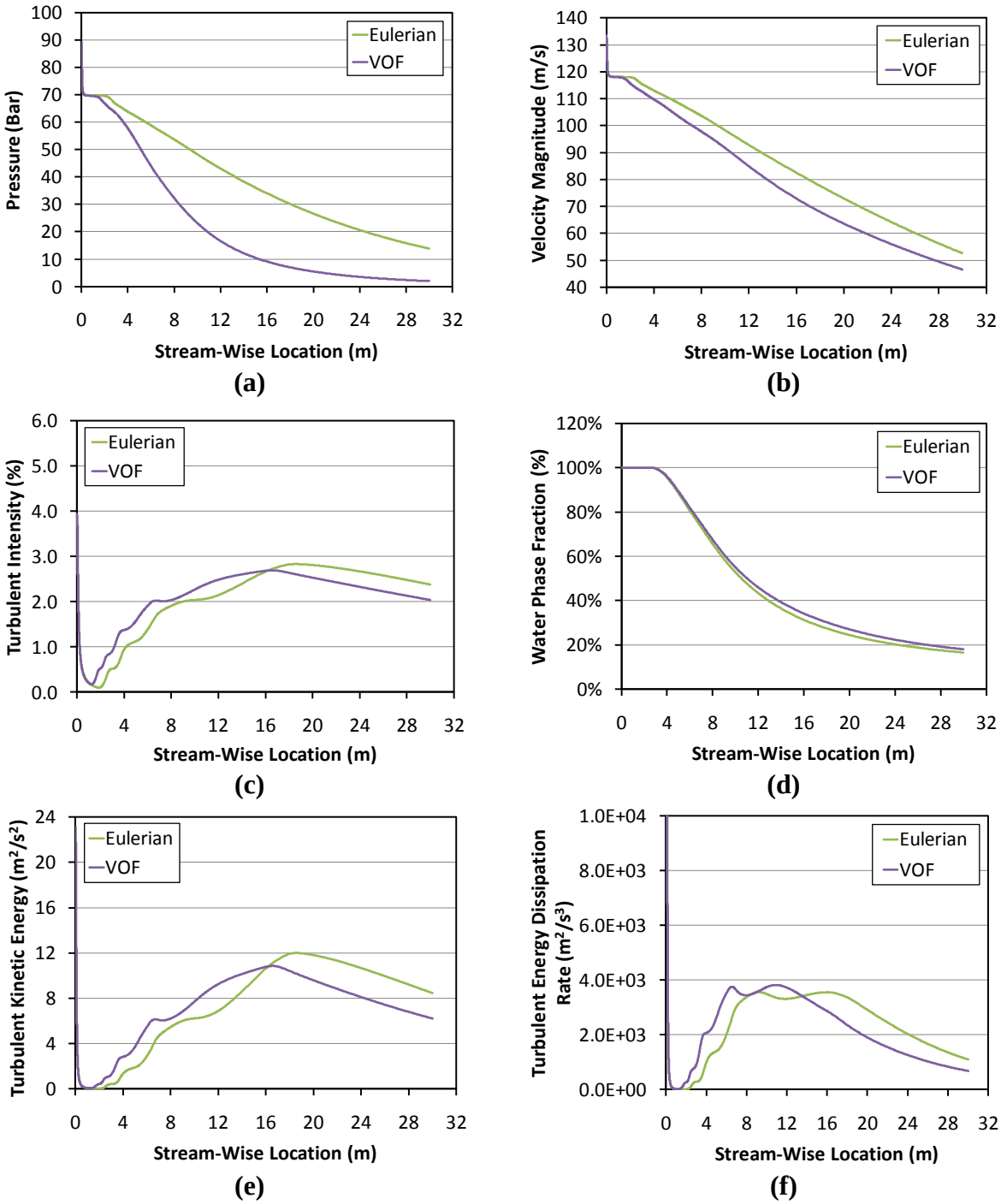

Figure 23. CFD Sub-Model Study: Multiphase Model Variation Along the Jet Centerline Showing (a) Pressure (b) Velocity Magnitude (c) Turbulent Intensity (d) Water Phase Fraction (e) Turbulent Energy Dissipation and (f) Turbulent Energy Dissipation Rate as a Function Of Stream-Wise Location From the Nozzle Exit

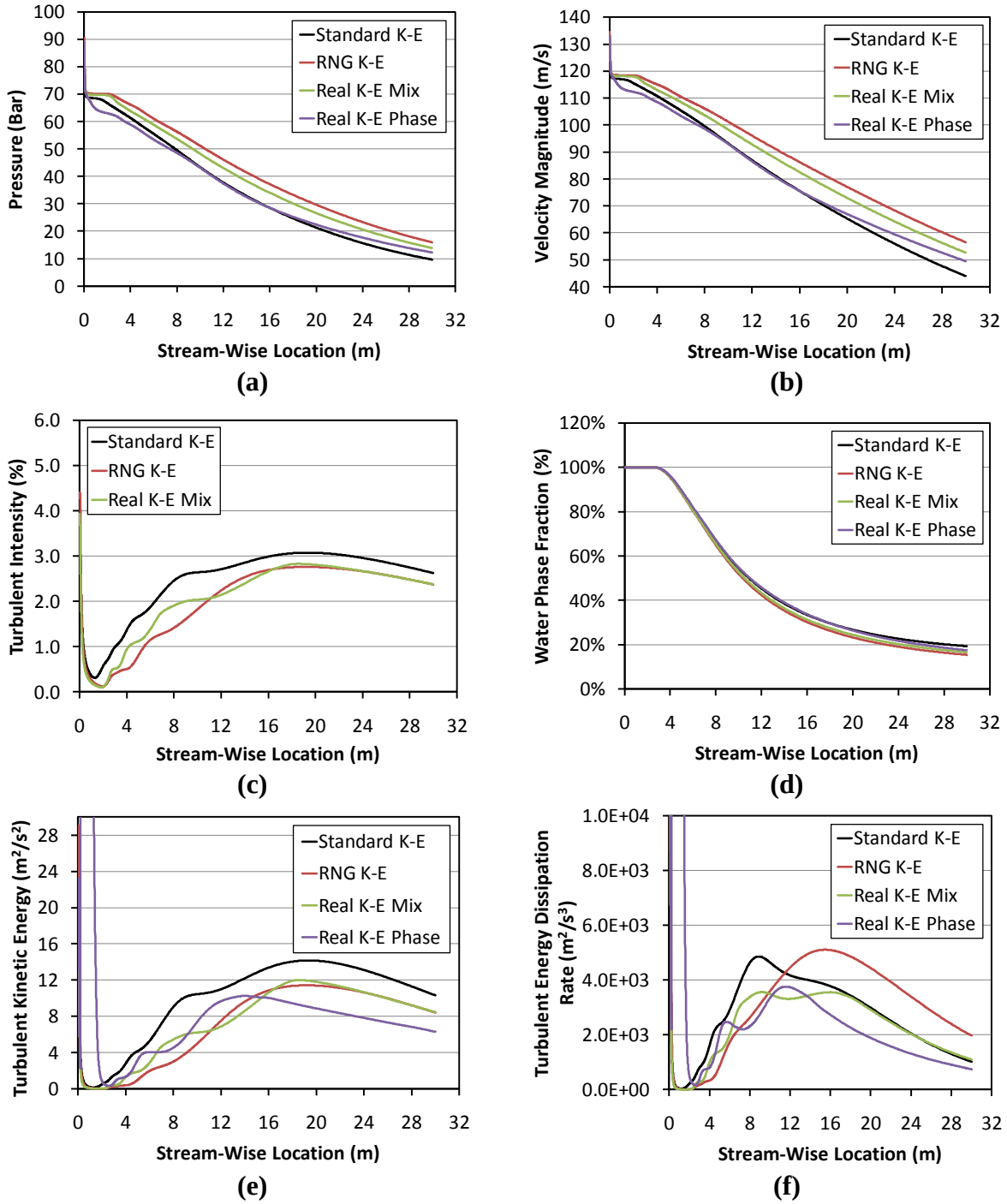

Figure 24. CFD Sub-Model Study: Turbulence Model Variation Along the Jet Centerline Showing (a) Pressure (b) Velocity Magnitude (c) Turbulent Intensity (d) Water Phase Fraction (e) Turbulent Energy Dissipation and (f) Turbulent Energy Dissipation Rate as a Function of Stream-Wise Location From the Nozzle Exit

Population balance (PB) droplet interaction dynamics were considered to account for both droplet aggregation and break-up (PB – All), aggregation only (PB – Agg), break-up only (PB – Brk), as well as no interaction (PB – None) at all but tracking of a non-uniform droplet diameter distribution. A Rossin-Ramler distribution ranging from 10 to 160 μm spanning seven discrete particle bins was initialized and tracked throughout the flow field, and previously tabulated in Table 1. The baseline condition was a non-interacting (constant) 10 μm droplet size. Figure 25 illustrates jet centerline results. A similar trend compared to the parameterized constant droplet size study was exhibited showing flow field pressure and velocity increase via the presence of larger, or aggregating particle families, and conversely reduced by particle family break-up, or small constant size (baseline) particle groups. Particle break-up only physics compared nearly identical to no interaction mechanisms activated, representing the weak presence larger particles maintained compared to the rest of the domain primarily made up of smaller droplets along the jet centerline. Turbulent quantities were likewise differentiated by particle size corresponding to larger, or aggregating only particles channeling more energy from the large mean to smaller dissipative turbulent flow scales.

PB droplet interaction dynamics were further illustrated in Figure 26 and Figure 27 where flow field output parameters were compared between the constant 10 μm droplet baseline model and the PB aggregation and break-up model, respectively, via transverse cross-sections through the jet at incremental locations downstream. In general, it was observed that small constant droplet baseline jet dynamics reveal more lateral dispersion compared to the PB model taking non-uniform droplet interaction dynamics into account for all observed conditions. Further inference can be found in Figure 28 where different PB interaction mechanics were compared to one another. Here, droplet diameter was plotted as a function of transverse location for the same cross-sectional jet stations. With the PB aggregation and break-up model both activated (Figure 28a), large droplets congregate closer to the jet centerline while smaller droplets disperse outward. In addition, a net droplet aggregation affect dominates the flow field as distance from the nozzle increases. With the PB no aggregation / no break-up (redistribution only) model activated (Figure 28b), larger droplets tend to disperse outward with smaller droplets concentrating closer to the jet centerline. The PB aggregation only model (Figure 28c) shows net droplet aggregation growth as downstream location from the nozzle increases as expected. Conversely, the PB break-up only model (Figure 28d) shows droplet size reduction as downstream nozzle locations increases, another anticipated result.

Variable droplet drag laws were also analyzed which provide varied descriptions of primary and secondary phase interaction based upon a variety of factors, most of which were empirical relations involving strong functions of local Reynolds number and droplet diameter. The Morsi-Alexander, Schiller-Naumann, universal, and symmetric drag laws were considered for this study, with the universal drag law implemented as the baseline condition. Figure 29 depicts the calculated results along the jet centerline. In general, all drag laws behave very similar to one another throughout the flow field, indicating jet centerline Reynolds number does not vary significantly along the length of the calculated physical domain.

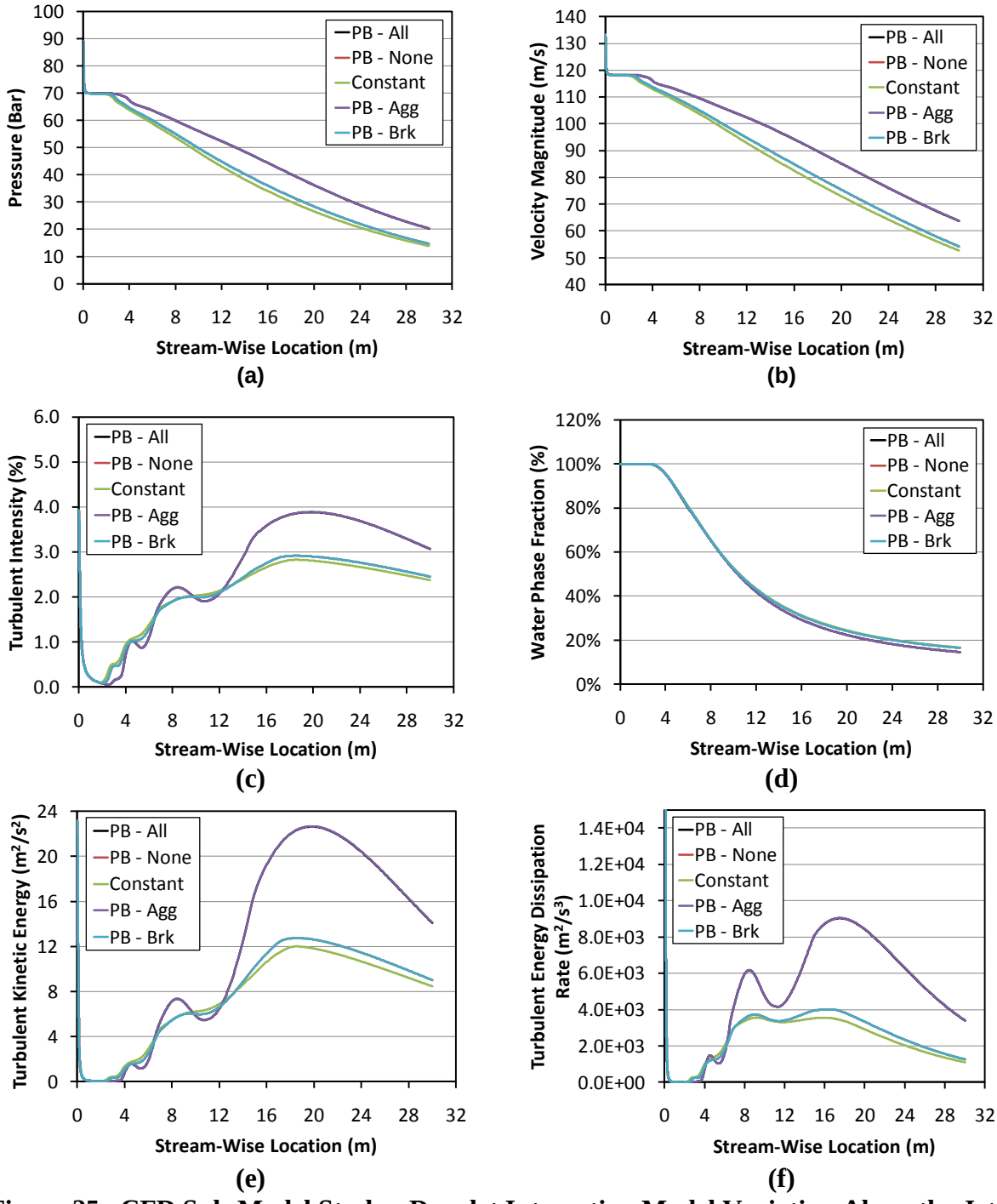

Figure 25. CFD Sub-Model Study: Droplet Interaction Model Variation Along the Jet Centerline Showing (a) Pressure (b) Velocity Magnitude (c) Turbulent Intensity (d) Water Phase Fraction (e) Turbulent Energy Dissipation And (f) Turbulent Energy Dissipation Rate as a Function of Stream-Wise Location From the Nozzle Exit

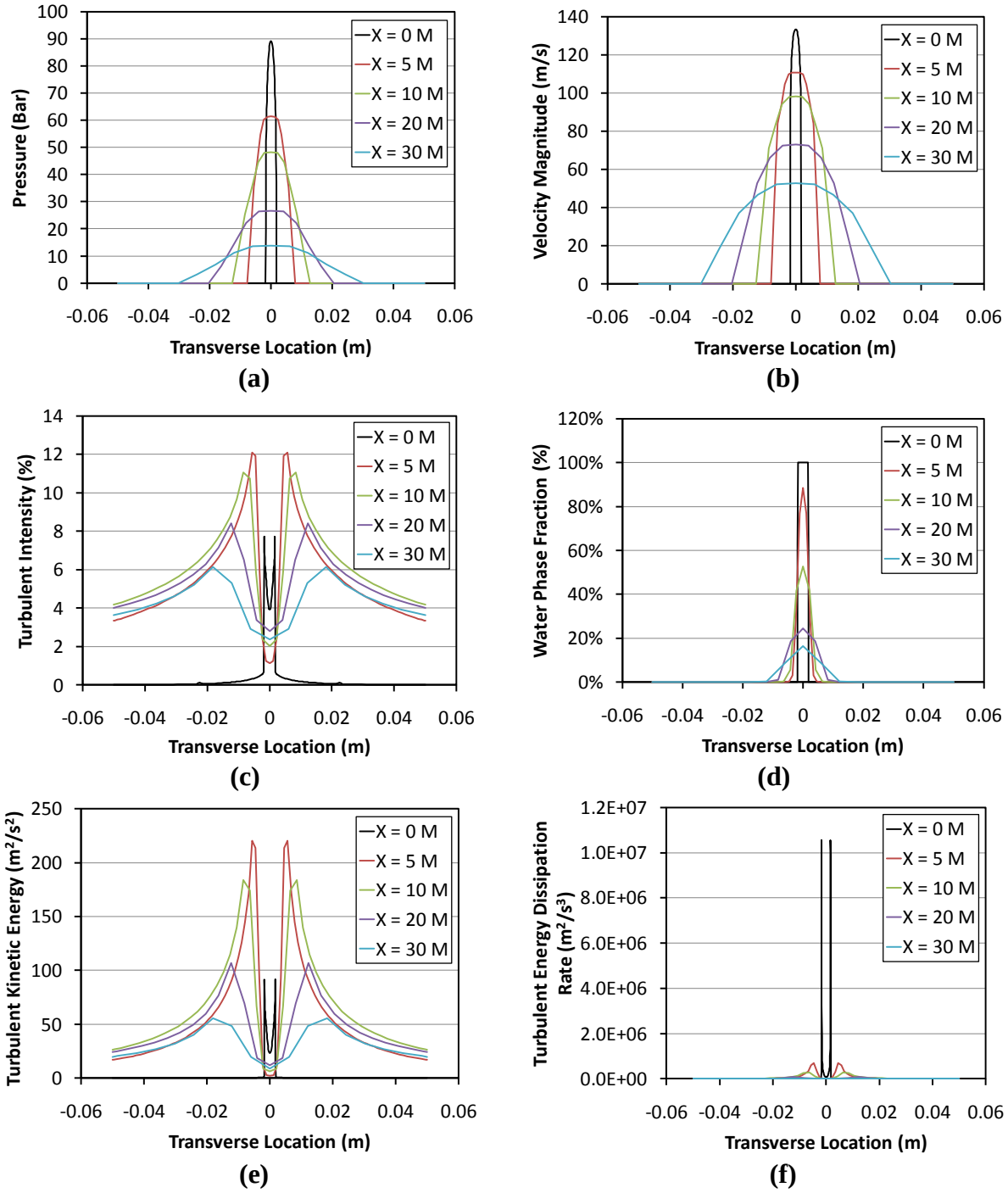

Figure 26. CFD Sub-Model Study: Baseline Model Comparing Variation Along Transverse Jet Cross-Sections Showing (a) Pressure (b) Velocity Magnitude (c) Turbulent Intensity (d) Water Phase Fraction (e) Turbulent Energy Dissipation and (f) Turbulent Energy Dissipation Rate as a Function of Transverse Location from the Jet Centerline

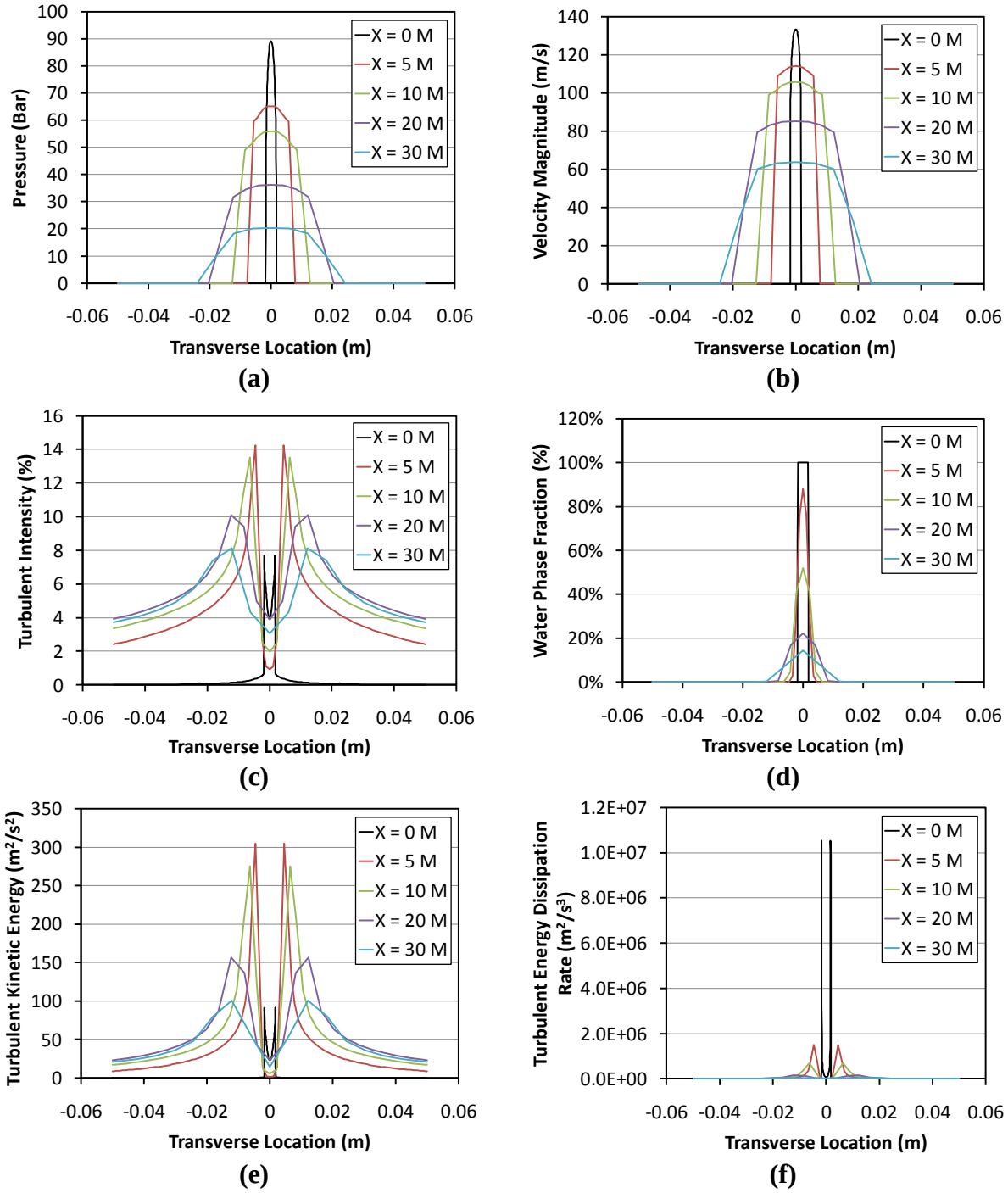

Figure 27. CFD Sub-Model Study: PB Aggregation / Break-Up Droplet Interaction Model Comparing Variation Along Transverse Jet Cross-Sections Showing (a) Pressure (b) Velocity Magnitude (c) Turbulence Intensity (d) Water Phase Fraction (e) Turbulent Kinetic Energy and (f) Energy Dissipation Rate as a Function of Transverse Location from the Jet Centerline

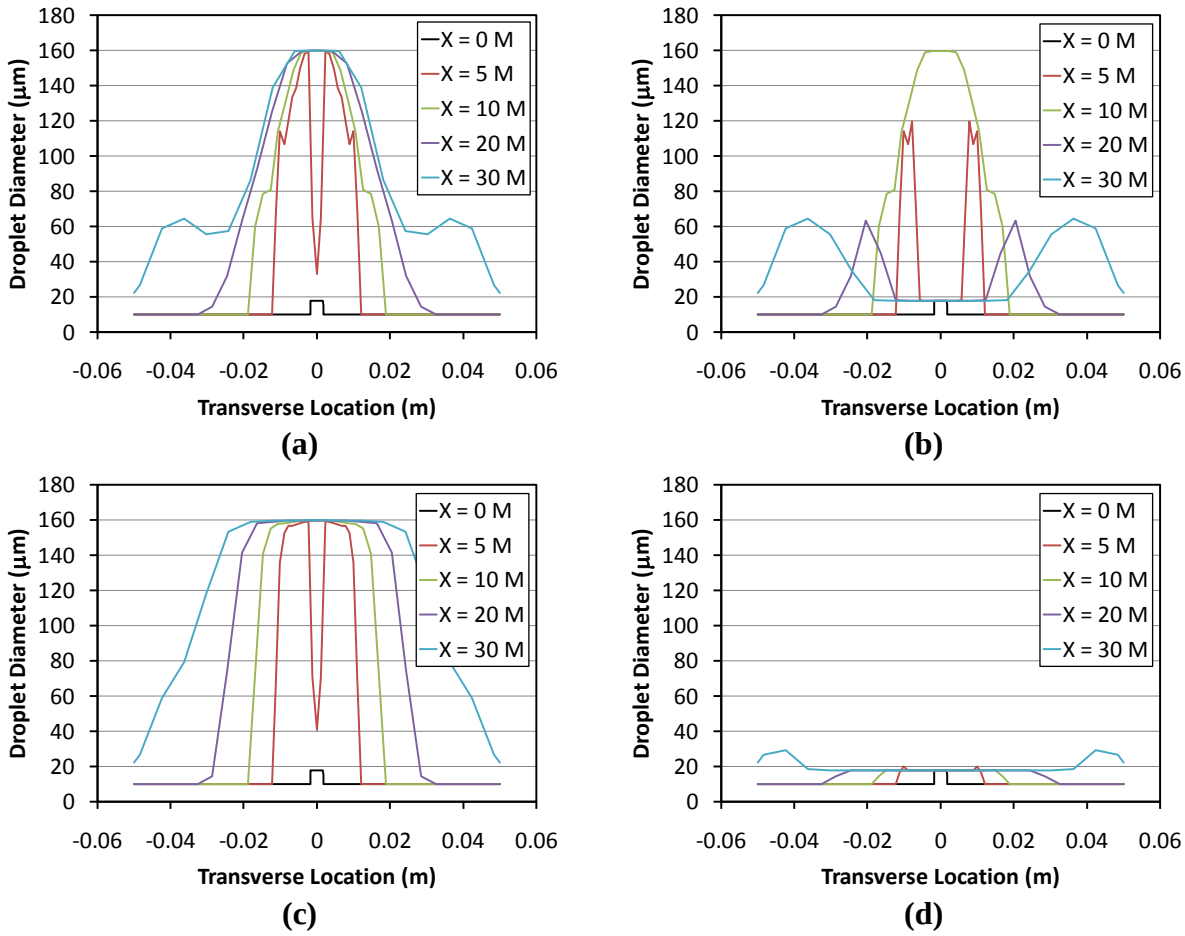

Figure 28. CFD Sub-Model Study: PB Droplet Interaction Model Comparing Transverse Jet Cross-Sections Showing Droplet Diameter Variation for the (a) PB Aggregation / Break-Up (b) No Aggregation / No Break-Up (c) PB Aggregation Only and (d) PB Break-Up Only Model as a Function of Transverse Location from the Jet Centerline

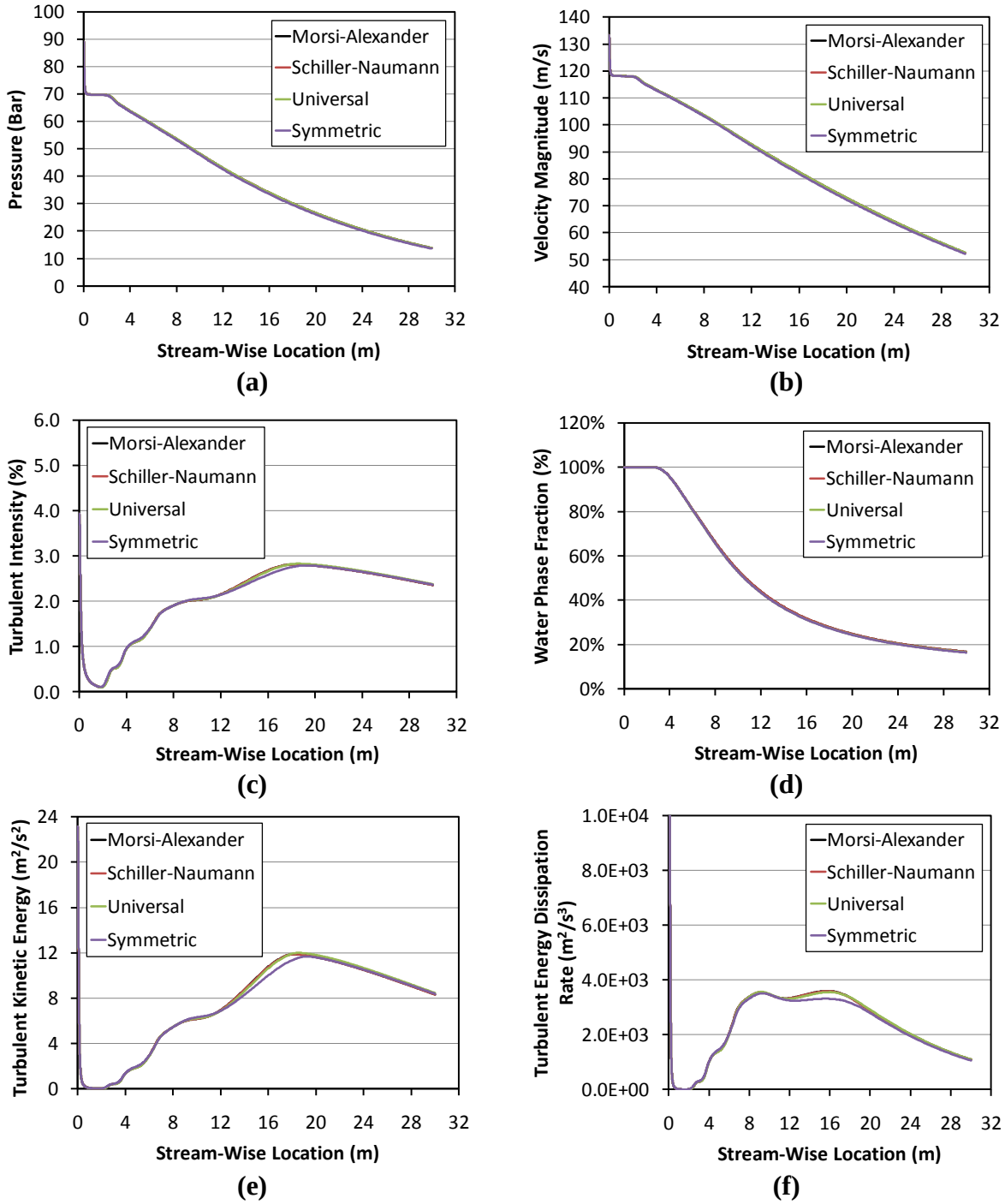

Figure 29. CFD Sub-Model Study: Droplet Drag Law Model Variation Showing (a) Pressure (b) Velocity Magnitude (c) Turbulence Intensity (d) Water Phase Fraction (e) Turbulent Kinetic Energy and (f) Turbulent Energy Dissipation Rate as a Function of Stream-Wise Location from the Nozzle Exit

5.5. Co-Flow Augmented Nozzle Study

To apply CFD modeling techniques as an optimization tool, an augmented co-flow nozzle concept was studied to determine if an energized annulus of air surrounding the nozzle exiting liquid core can substantially extend the reach of a UHP jet. The basis of this theory lies in an attempt to reduce the shear stress imparted by the stagnant atmosphere surrounding the agent as it exits the nozzle at high velocity. With a shroud of air moving at the same velocity as the liquid core, viscous losses were reduced conserving agent momentum in the mean spray direction. The inner liquid core geometry was identical to the straight bore baseline nozzle concept, with the co-flow air shroud sized to inject the same amount of momentum at the nozzle exit plane relative to agent injection into the atmosphere. Air shroud velocities were tuned to minimize the shear between the agent and air phases.

Figure 30 and Figure 31 illustrate the agent and air phase velocities in the near field of the nozzle exit, respectively. Although the agent velocity was well preserved, the air shroud velocity dissipated quickly within the first few nozzle diameters due to rapid momentum diffusion. Conversely, the agent jet momentum stayed relatively well-preserved due to its comparatively much higher fluid density. Figure 32 depicts the relatively rapid decline of total agent pressure as it varies non-linearly with respect to local velocity. Figure 33 shows a typical phase fraction plot distinguishing the agent from the air phase, identifying both phase regimes. Figure 34 and Figure 35 depict the influence of turbulence in the co-flow nozzle near field, showing areas of increased turbulent energy exchange between the two fields combining to create a region of high shear just above the air shroud. Although these effects were felt downstream, their global impact on the flow field degrades quickly and was nearly negligible further downstream. Figure 36 illustrates jet centerline output parameters reflecting a global minute offset between baseline and co-flow nozzle results.

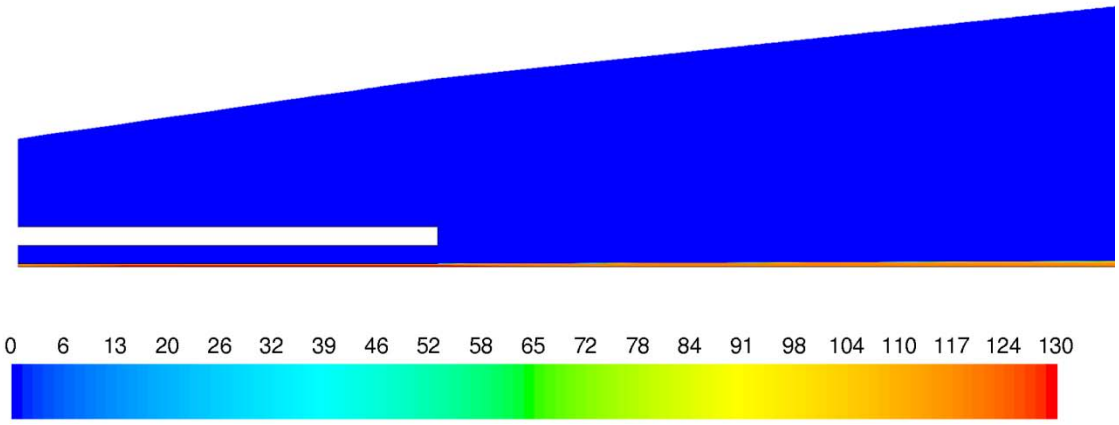

Figure 30. Near Field Water Phase Velocity (m/s) Contours of the Co-flow Nozzle

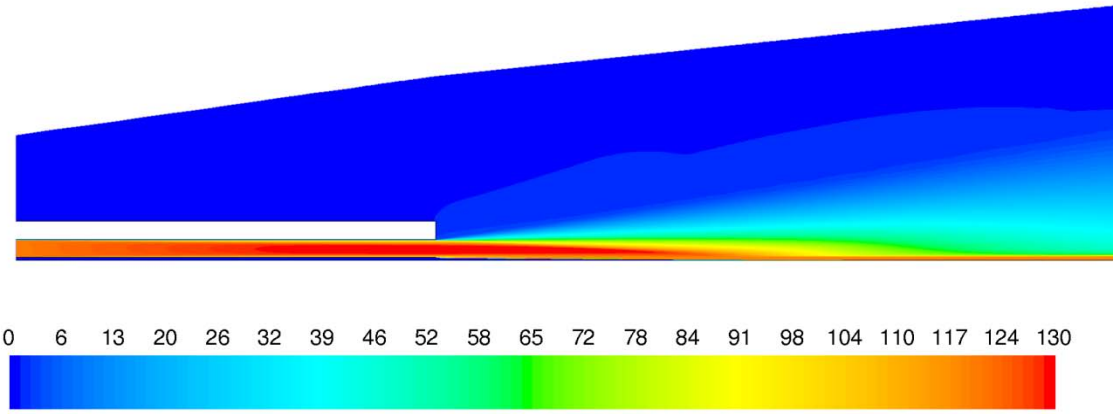

Figure 31. Near Field Air Phase Velocity (m/s) Contours of the Co-flow Nozzle

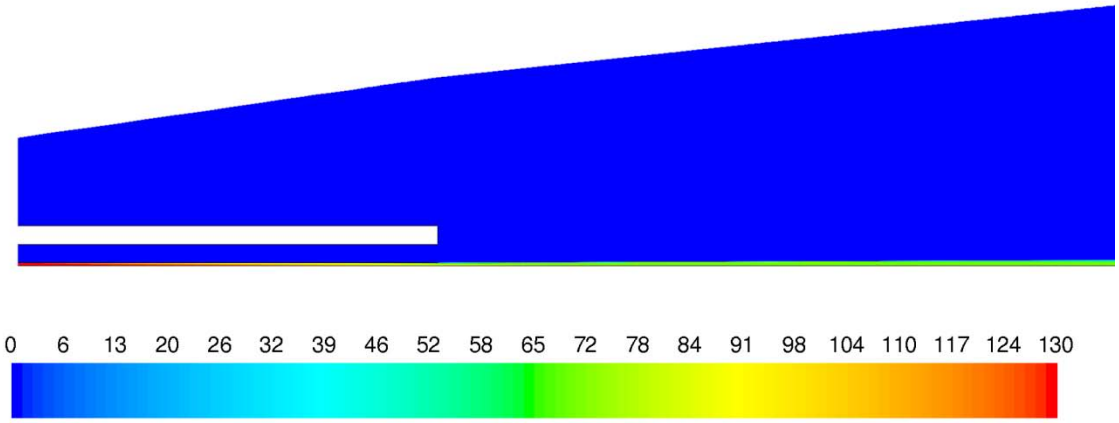

Figure 32. Near Field Water Phase Total Pressure (bar) Contours of the Co-flow Nozzle

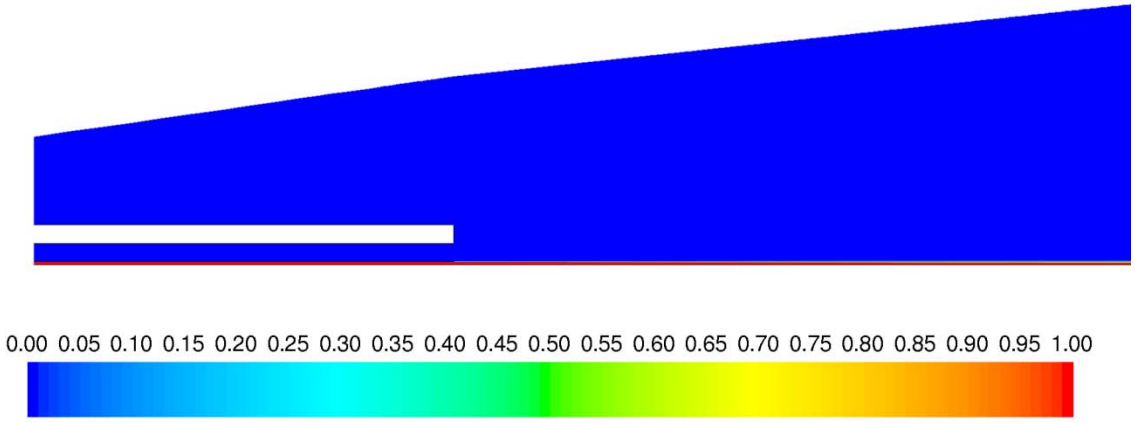

Figure 33. Near Field Water Phase Volume Fraction (%) Contours of the Co-flow Nozzle

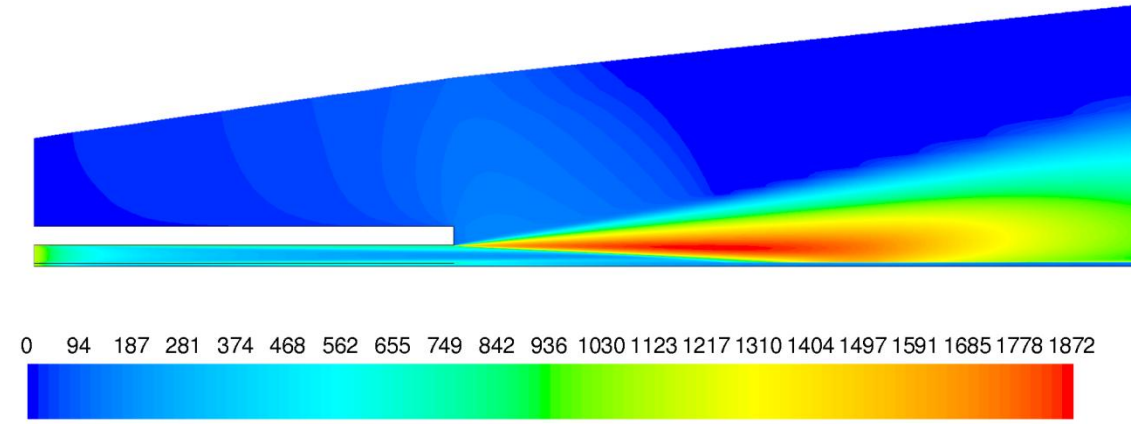

Figure 34: Near Field Turbulence Intensity (%) Contours of the Co-flow Nozzle

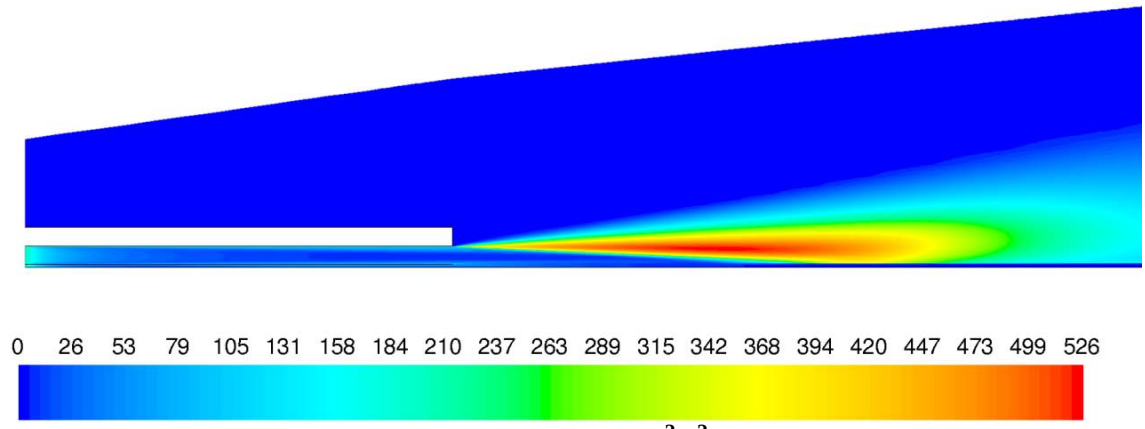

Figure 35. Near Field Turbulent Kinetic Energy (m^2/s^2) Contours of the Co-flow Nozzle

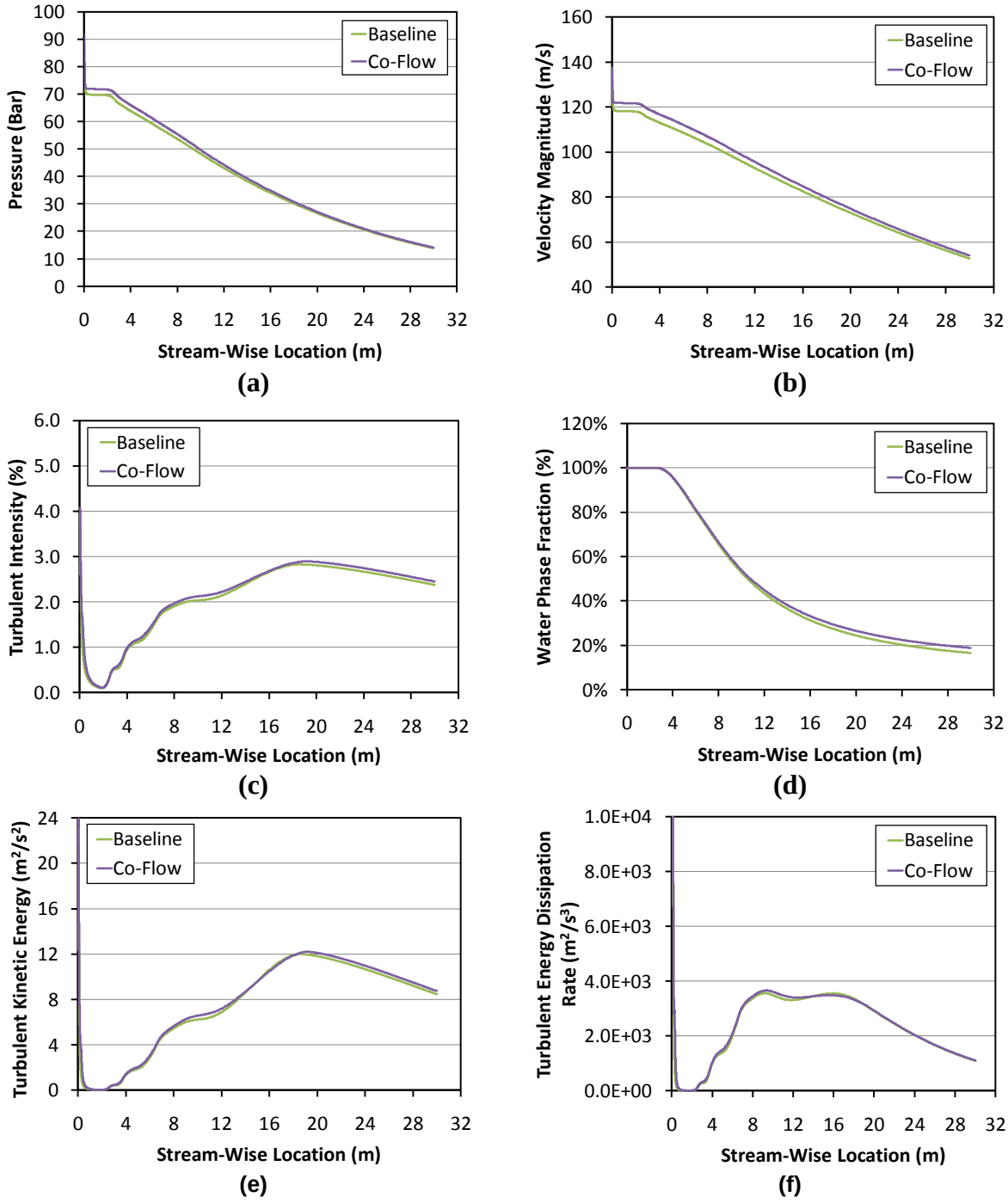

Figure 36. Nozzle Concept Variation Showing (a) Pressure (b) Velocity Magnitude (c) Turbulent Kinetic Energy (d) Water Phase Fraction (e) Turbulent Kinetic Energy and (f) Turbulent Energy Dissipation Rate as a Function of Stream-Wise Location from the Nozzle Exit

6.0 CONCLUSIONS

6.1. Experimental LDV/PDPA Field Sampling Conclusions

Experimental LDV and PDPA field sampling was successfully conducted using equipment from two commercial manufacturers to measure UHP stream dynamics with and without the addition of AFFF. Although flow regimes in the very near and far fields of the UHP jet approached equipment DAQ thresholds, signal-to-noise ratios in these vicinities were deemed acceptable with no major alterations needed to capture quality flow statistics. Droplet distribution ranges coupled with velocity trend and magnitude analysis provided practical insight and approximate boundary conditions for the initial development and deployment of agent application CFD models.

6.2. Computational Flow Modeling Conclusions

A parametric computational flow analysis was conducted examining several aspects of the UHP jet transport process, including fluid transport, fluid property, as well as CFD sub-model approximations. In addition, modeling efforts were extended to analyze a co-flow nozzle concept to determine its viability as a practical application to extend UHP jet reach.

All reported results reflect the output of 2-D axisymmetric solutions. Because of this, gravitational effects were not taken into account. In addition, 3-D effects were also neglected to reduce computational overhead, together partially limiting the applicability of this work. Modeling techniques were selected based upon the best applicability to all parameters and physical environment examined. Alternative methods may provide better results for more specific flow regimes of interest. Due to the absence of extensive experimental data to validate computational results, conclusions should be considered preliminary in nature with more detailed investigations required for further deliberation.

From a nozzle flow condition perspective, it was found that higher exit pressures, larger droplet sizes, and higher flow rates aid in extending UHP jet reach. However, significant nozzle discharge pressures and droplet diameter increases depicted marginal gains compared to an increase in flow rate. Keeping agent momentum and fluid state properties constant, higher flow rates demand larger discharge areas that correspond to a thickened liquid jet core exiting the nozzle. This thickened liquid core created a longer residence time for the coherent agent stream to stay intact while its exterior was diffused into the air, ultimately extending the range of the jet. Nozzle discharge turbulence intensity variation had a negligible effect on downstream jet performance, indicating agent-air mixing was the dominant source of turbulent production for smooth straight bore nozzles.

From a fluid property standpoint, it was observed that higher agent densities and lower viscosities extend UHP jet reach. This corresponds to an increase in jet Reynolds number, whereby inertial jet forces dominate viscous forces. The sensitivity of UHP jet characteristics to Reynolds number dependence was addressed by altering agent dynamic viscosity over two orders of magnitude and agent density relatively slightly. Agent surface tension effects chosen over an applicable range of interest showed negligible change in UHP jet performance due to

large Weber numbers, corresponding to inertial forces dominating over surface tension forces as well.

From a CFD sub-model position, it was found that the Eulerian and VOF model faired similarly both trend and magnitude-wise, except substantial differences were found in the pressure decay rate revealing the need for further investigation. This discrepancy also supports the need for thorough experimental data collection to compare model results throughout the flow field, and not just at upstream near field nozzle locations.

Turbulence model variation showed no significant differences within the k-ε family, but enough to explore alternative turbulence model formulations to better interpret broad effects of turbulent flow. Because two-equation linear eddy viscosity models like the k-ε model are isotropic in nature, confidence in these models increase as jet Reynolds number increases, and conversely decrease at lower jet Reynolds numbers where transitionally turbulent flow structures are more anisotropic. In these lower Reynolds number regimes, more complex turbulent models may be required to capture appropriate flow physics.

Non-uniform droplet interaction dynamics via PB methods provide feedback depicting how evolving droplet sizes affect global UHP jet characteristics. In general, both PB aggregation and break-up models reported physically expected results, trending droplet growth and decay in appropriate directions depending upon model implementation and interaction. Further work is required to determine what droplet interaction models dominate actual UHP flow fields, and to what degree. Major flow output parameters showed little dependency on varying the droplet drag law, alluding to similar Reynolds number maintenance throughout the flow field making functional drag effects negligible between applied models.

Finally, a co-flow nozzle concept was examined to determine if augmenting the flow field around the near field of the nozzle exit would enhance UHP jet reach. CFD model predictions dictate a negligible impact was felt downstream because of rapid momentum diffusion about the air annulus. Although this work concludes a steady co-flow nozzle may be an unlikely candidate to significantly extend UHP jet reach, transient applications coupled with higher fidelity model approximations may prove otherwise.

6.3. Recommendations

Rigorous experimental flow characterization should be conducted to fully detail a sample UHP jet and gain more insight into the agent transport process, as well as provide validation data for more sophisticated computational models. Empirical analysis should also extend to higher flow rates to discern the absolute upper bound of LDV/PDPA systems. In addition, alternative experimental methods should be explored to better quantify flow physics at higher flow rates where LDV/PDPA methods are inapplicable.

To provide a more thorough description of the agent stream, computational modeling efforts should be extended to 3-D environments where gravitational effects can be accounted for, especially in denser flow regimes where body forces cannot be considered negligible. Time resolved computations should also be examined to determine sensitivity to unsteady effects, as

well as provide a complete explicit description of the liquid jet break-up process via auxiliary models such as VOF.

Alternative multiphase models capable of integrating into a combustion framework like DPM should also be explored to begin building solution strategies involving a complete agent application / fire suppression event.

In addition, other nozzle concepts such as a pulsed agent stream or a pulsed co-flow UHP jet should be analyzed where transient effects may have greater positive impact, potentially providing improved performance over the steady co-flow nozzle examined in this study.

7.0 REFERENCES

1. McDonald, M.J., Dierdorf, D.S., Kalberer, J.L., and Barrett, K.D. "Fire Extinguish Effectiveness Tests." Defense Technical Information Center. AFRL-ML-TY-TR-2004-4554. Final Technical Report: October 2005.

2. Menchini, C.P. Dierdorf, D.S., and Kalberer, J.L. "The Development and Design of a Prototype Ultra High Pressure P-19 Firefighting Vehicle." Defense Technical Information Center. AFRL-ML-TY-TR-2007-4525. Final Technical Report: February 2007.

3. NFPA 412: "Standard for Evaluating Aircraft Rescue and Firefighting Foam Equipment." National Fire Protection Association (NFPA). 2003 Edition.

4. Grosskopf, K.R. and Kalberer, J.L. "Potential Impacts of Ultra High Pressure (UHP) Technology on NFPA Standard 403." Fire Safety Journal 43 (2008): 308-315.

5. Theobald, C. "The Effect of Nozzle Design on the Stability and Performance of Turbulent Water Jets." Fire Safety Journal 4 (1981): 1-13.

6. McCarthy, M.J. and Molloy, N.A. "Review of Stability of Liquid Jets and the Influence of Nozzle Design." Chemical Engineering Journal 7 (1974): 1-20.

7. Husted, B.P., Petersson, P., Lund, I., and Holmstedt, G. "Comparison of PIV and PDA Droplet Velocity Measurement Techniques on Two High-Pressure Water Mist Nozzles." Fire Safety Journal 44 (2009): 1030-1045.

8. Yoon, S.S., Kim, H.Y., and Hewson, J.C.. "Effect of Initial Conditions of Modeled PDFs on Droplet Characteristics for Coalescing and evaporating Turbulent Water Spray Used in Fire Suppression Applications." Fire Safety Journal 42 (2007): 393-406.

9. Yoon, S.S. "Droplet Distributions at the Liquid Core of a Turbulent Spray. Physics of Fluids 17 (2005). 035103.

10. Park, H., Yoon, S.S., Heisyer, S.D. "A Non-linear atomization Model for Computation of Drop-size Distributions and Complete Spray Simulation." International Journal of Numerical Methods in Fluids 48 (2005): 1219-1240.

11. Dantec Dynamics. "Laser Doppler Anemometry." 5 January 2010. http://www.dantecdynamics.com.

12. TSI, Inc. "Phase Doppler Particle Analysis." 5 January 2010. http://www.tsi.com.

13. Young, D.F., Munson, B.R., and Okiishi, T.H. "A Brief Introduction to Fluid Mechanics." New York: John Wiley & Sons, Inc., 1997.

14. Versteeg, H.K. and Malalasekera, W. “An Introduction to Computational Fluid Dynamics: The Finite Volume Method.” 2nd Ed. London: Prentice Hall, 2007.

15. ANSYS, Inc. “ANSYS Fluent 12 Theory Guide.” 5 January 2010. http://www.ansys.com.

16. ANSYS, Inc. “ANSYS Fluent 12 Population Balance Guide.” 5 January 2010. http://www.ansys.com.

APPENDIX A. BASELINE CFD CASE SUMMARY

FLUENT
Version: axi, dp, pbns, Eulerian, rke
(axi, Double Precision, Pressure-based, Eulerian, Realizable k-epsilon)
Release: 12.1.2

Models

Model	Settings
Space	Axisymmetric
Time	Steady
Viscous	Realizable k-epsilon turbulence model
Wall Treatment	Standard Wall Functions
Multiphase	k-epsilon Models Mixture k-epsilon
Heat Transfer	Enabled
Solidification and Melting	Disabled
Radiation	None
Species Transport	Disabled
Coupled Dispersed Phase	Disabled
Pollutants	Disabled
Pollutants	Disabled
Soot	Disabled

Material Properties

Material: water-liquid (fluid)

Property	Units	Method	Value(s)
Density	kg/m3	Constant	1000
Cp (Specific Heat)	j/kg-k	Constant	4182
Thermal Conductivity	w/m-k	Constant	0.600
Viscosity	kg/m-s	Constant	0.001003
Molecular Weight	kg/kgmol	Constant	18.0152
Standard State Enthalpy	j/kgmol	Constant	-2.858e+08
Reference Temperature	k	Constant	298
Thermal Expansion Coefficient	1/k	Constant	0
Speed of Sound	m/s	Cone	N/A

Material: air (fluid)

Property	Units	Method	Value(s)
Density	kg/m3	Incomp-ideal-gas	N/A
Cp (Specific Heat)	j/kg-k	Constant	1006.43
Thermal Conductivity	w/m-k	Constant	0.0242
Viscosity	kg/m-s	Constant	1.7894e-05
Molecular Weight	kg/kgmol	Constant	28.966
Standard State Enthalpy	j/kgmol	Constant	0
Reference Temperature	k	Constant	298.14999
Thermal Expansion Coefficient	1/k	Constant	0
Speed of Sound	m/s	None	N/A

Boundary Conditions

Zones

Name	Type
Nozzle-Inlet	Pressure-inlet
Nozzle	Wall
Axis	Axis
Pressure-outlet	Pressure-outlet
Pressure-inlet	Pressure-inlet

Setup Conditions

Nozzle-inlet

Condition	Value(s)
Reference Frame	0
Gauge Total Pressure (atm)	130
Supersonic/Initial Gauge Pressure (atm)	0
Direction Specification Method	1
Coordinate System	0
Turbulent Specification Method	3
Turbulent Kinetic Energy (m2/s2)	1
Turbulent Dissipation Rate (m2/s3)	1
Turbulent Intensity (%)	10
Turbulent Length Scale (m)	1
Hydraulic Diameter (m)	0.0035
Turbulent Viscosity Ratio	10
Is Zone Used In Mixing-Plane Model?	No

Nozzle

Condition	Value(s)
Wall Thickness (m)	0
Heat Generation Rate (w/m3)	0
Material Name	Aluminum
Thermal BC Type	1
Temperature (k)	300
Heat Flux (w/m2)	0
Convective Heat Transfer Coefficient (w/m2-k)	0
Free Stream Temperature (k)	300
Wall Motion	0
Shear Boundary Condition	0
Define Wall Motion Relative to Adjacent Cell Zone?	Yes
Apply a Rotational Velocity to this Wall?	No
Velocity Magnitude (m/s)	0
X-Component of Wall Translation	1
Y-Component of Wall Translation	0
Define Wall Velocity Components?	No
X-Component of Wall Translation (m/s)	0
Y-Component of Wall Translation (m/s)	0
External Emissivity	1
External Radiation Temperature (k)	300
Wall Roughness Height (m)	0
Wall Roughness Constant	0.5
Rotation Speed (rad/s)	0
X-component of Shear Stress (atm)	0
Y-component of Shear Stress (atm)	0
Surface Tension Gradient (n/m-k)	0
Specularity Coefficient	0

Axis

Condition	Value(s)
Not Applicable	

Pressure-outlet

Condition	Value(s)
Gauge Pressure (atm)	0
Backflow Direction Specification Method	1
Turbulent Specification Method	3

Backflow Turbulent Kinetic Energy (m2/s2)	1
Backflow Turbulent Dissipation Rate (m2/s3)	1
Backflow Turbulent Intensity (%)	10
Backflow Turbulent Length Scale (m)	1
Backflow Hydraulic Diameter (m)	0.0035
Backflow Turbulent Viscosity Ratio	10
Is Zone Used In Mixing-plane Model?	No

Pressure-inlet

Condition	Value(s)
Reference Frame	0
Gauge Total Pressure (atm)	0
Supersonic/Initial Gauge Pressure (atm)	0
Direction Specification Method	1
Coordinate System	0
Turbulent Specification Method	3
Turbulent Kinetic Energy (m2/s2)	1
Turbulent Dissipation Rate (m2/s3)	1
Turbulent Intensity (%)	10
Turbulent Length Scale (m)	1
Hydraulic Diameter (m)	0.0035
Turbulent Viscosity Ratio	10
Is Zone Used In Mixing-plane Model?	No

Solver Settings

Equations

Equation	Solved
Flow	Yes
Volume Fraction	Yes
Turbulence	Yes
Energy	Yes

Numerics

Numeric	Enabled
Absolute Velocity Formulation	Yes

Relaxation

Variable	Relaxation Factor
Density	1
Body Forces	1
Volume Fraction	0.5
Turbulent Kinetic Energy	0.8
Turbulent Dissipation Rate	0.8
Turbulent Viscosity	1
Energy	1

Linear Solver

Variable	Solver Type	Termination Criterion	Residual Reduction Tolerance
Flow	F-Cycle	0.1	
Volume Fraction	Flexible	0.1	0.7
Turbulent Kinetic Energy	Flexible	0.1	0.7
Turbulent Dissipation Rate	Flexible	0.1	0.7
Energy	Flexible	0.1	0.7

Pressure-Velocity Coupling

Parameter	Value(s)
Type	Multiphase Coupled
Courant Number	200
Explicit Momentum Relaxation Factor	1
Explicit Pressure Relaxation Factor	1

Discretization Scheme

Variable	Scheme
Momentum	Second Order Upwind
Volume Fraction	QUICK
Turbulent Kinetic Energy	Second Order Upwind
Turbulent Dissipation Rate	Second Order Upwind
Energy	Second Order Upwind

Solution Limits

Quantity	Limit
Minimum Absolute Pressure	1
Maximum Absolute Pressure	5e+10
Minimum Temperature	1
Maximum Temperature	5000
Minimum Turb. Kinetic Energy	1e-14
Minimum Turb. Dissipation Rate	1e-20
Maximum Turb. Viscosity Ratio	100000

LIST OF ABBREVIATIONS AND ACRONYMS

Abbreviations	Description
1-D	One-Dimensional
2-D	Two-Dimensional
3-D	Three-Dimensional
L/D	Nozzle Length to Diameter Ratio
Re	Reynolds Number
We	Weber Number
Q	Volumetric Flow Rate

Acronyms	Description
AFB	Air Force Base
AFRL	Air Force Research Laboratory
ARFF	Aircraft Rescue Firefighting
AFFF	Aqueous Film-Forming Foam
CFD	Computational Fluid Dynamics
DAQ	Data Acquisition
DPM	Discrete Phase Model
DDPM	Dense Discrete Phase Model
FRE	First Response Expeditionary Vehicle
LDV	Laser Doppler Velocimetry
NFPA	National Fire Protection Association
PB	Population Balance
PDF	Probability Density Function
PDPA	Phase Doppler Particle Analysis
PIV	Particle Image Velocimetry
RANS	Reynolds Averaged Navier-Stokes
RMS	Root Mean Square
RXQD	Fire Research Team
UHP	Ultra High Pressure
USAF	United States Air Force
VOF	Volume of Fluid